

1 The sensitivity of primary productivity in
2 Disko Bay, a coastal Arctic ecosystem to
3 changes in freshwater discharge and sea
4 ice cover
5

6 Eva Friis Møller¹, Asbjørn Christensen², Janus Larsen¹, Kenneth D. Mankoff^{3,4,5}, Mads Hvid
7 [Ribergaard](#)⁵[Ribergaard](#)⁶, Mikael Sejr¹, Philip ~~Wallhead~~⁶[Wallhead](#)⁷, Marie Maar¹

Formatted: Superscript

8 ¹Department of Ecoscience, Aarhus University, 4000 Roskilde, Denmark

9 ²DTU Aqua, Technical University of Denmark, DK-2880 Kgs. Lyngby, Denmark

10 ³Department of Glaciology and Climate, Geological Survey of Denmark and Greenland, 1350
11 Copenhagen, Denmark

12 ⁴~~National Snow and Ice Data Center (NSIDC), Cooperative Institute for Research in
13 Environmental Sciences (CIRES), University of Colorado Boulder, Boulder, CO, 80390, USA~~

14 ⁵~~Danish~~⁴[Business Integra, New York, NY, USA](#)

15 ⁵[NASA Goddard Institute for Space Studies, New York, NY, USA](#)

16 ⁶[Danish](#) Meteorological Institute, 2100 Copenhagen, Denmark

17 ⁶~~Section~~⁷[Section](#) for Oceanography, Norwegian Institute for Water Research (NIVA Vest),
18 Bergen, Norway

19 *Correspondence to:* Eva Friis Møller (efm@ecos.au.dk)

20 **Abstract.** The Greenland Ice Sheet is melting, and the rate of ice loss has increased 6-fold since
21 the 1980s. At the same time, the Arctic sea ice extent is decreasing. Melt water runoff and sea ice
22 reduction both influence light and nutrient availability in the coastal ocean with implications for
23 the timing, distribution and magnitude of phytoplankton production. However, the integrated
24 effect of both glacial and sea ice melt is highly variable in time and space, making it challenging
25 to quantify. In this study, we evaluate the relative importance of these processes for the primary
26 productivity of Disko Bay, West Greenland, one of the most important areas for biodiversity and
27 fisheries around Greenland. We use a high-resolution 3D coupled hydrodynamic-biogeochemical
28 model for 2004 to 2018 validated against *in situ* observations and remote sensing products. The
29 model estimated net primary production (NPP) varied between 90-147 gC m⁻² year⁻¹ during
30 2004-2018, a period with variable freshwater discharges and sea ice cover. NPP correlated
31 negatively with sea ice cover, and positively with freshwater discharge. Freshwater discharge
32 had a strong local effect within ~25 km of the source sustaining productive hot spot's during
33 summer. When considering the annual NPP at bay scale, sea ice cover was the most important
34 controlling factor. In scenarios with no sea ice in spring, the model predicted ~30% increase in
35 annual production compared to a situation with high sea ice cover. Our study indicates that
36 decreasing ice cover and more freshwater discharge can work synergistically and will likely
37 increase primary productivity of the coastal ocean around Greenland.

38 1 Introduction

39 The warming of the Arctic (Cohen et al., 2020) has a strong impact on the regional sea ice. Over
40 the past few decades, the sea ice melt season has lengthened (Stroeve et al., 2014), summer
41 extent has declined, and the ice is getting thinner (Meier et al., 2014). This has an immediate
42 effect on the primary producers of the ocean. The photosynthetic production is constrained by
43 the annual radiative cycle, and the sea ice reduces the availability of light and thereby the
44 development of the sea ice algae and the pelagic phytoplankton communities (Ardyna et al.,
45 2020). An extended open water period will affect the phenology of primary producers and
46 potentially lead to an earlier spring bloom (Ji et al., 2013; Leu et al., 2015), and may also
47 increase the potential for autumn blooms (Ardyna et al., 2014).

48 In the Arctic coastal ocean, there are additional impacts of a warming climate. As the freshwater
49 discharge increases due the melt of snow and ice on land and higher precipitation (Kjeldsen et
50 al., 2015; Mankoff et al., 2020a, 2021), the land-ocean coupling along the extensive Arctic
51 coastline is intensified (Hernes et al., 2021). The summer inflow of melt water has complex
52 biogeochemical impacts on the coastal ecosystem and combines with changes in sea ice cover to
53 affect the magnitude and phenology of marine primary production. In areas dominated by
54 glaciated catchments such as Greenland, the increase in melt water discharge has been
55 substantial and the rate of ice mass loss has increased sixfold since the 1980s (Mankoff et al.,
56 2020b; Mougnot et al., 2019).

57 The changes in sea ice cover and freshwater discharge will affect the marine primary production
58 through the complex interactions of changes in stratification, light and nutrient availability
59 (Arrigo and van Dijken, 2015; Hopwood et al., 2020). The individual processes are relatively
60 well described, but the interactions between them and the temporal and spatial importance under
61 different Arctic physical regimes are less well understood. A lower extent of sea ice cover may
62 also increase the wind-induced mixing of the water column and deepen or weaken the
63 stratification. Thereby, the potential for the phytoplankton to stay and grow in the illuminated
64 surface layer is reduced. At the same time, a higher mixing rate will increase the supply of new
65 nutrients from deeper layers to support production when light is not limiting (Tremblay and
66 Gagnon, 2009). Another mechanism affecting stratification is the freshening of the surface layer
67 due to ice melt from both sea ice and the ice sheet (von Appen et al., 2021; Holding et al., 2019).

68 If a glacier terminates in a deep fjord, the ice sheet melt is injected at depth causing more coastal
69 upwelling of nutrients (Hopwood et al., 2018; Meire et al., 2017)

70 The relative importance on productivity of sea ice versus glacier freshwater discharge depends
71 on the scale considered (Hopwood et al., 2019). Freshwater discharge from the ice sheet is more
72 important in the vicinity of the glacier (Hopwood et al., 2019; Meire et al., 2017), whereas the
73 sea ice dynamics are considered to be an important driver in the open ocean (Arrigo and van
74 Dijken, 2015; Massicotte et al., 2019; Meier et al., 2014). Most studies consider one or the other
75 separately (e.g. Hopwood et al., 2018; Vernet et al., 2021). However, in the coastal Arctic areas
76 at the mesoscale, i.e. 10-100 km, it can be expected that both sea ice and glacier freshwater
77 discharge and the interaction between them will influence the ecosystem and the pelagic primary
78 production (Hopwood et al., 2019). To resolve their relative impacts, we need to constrain their
79 impacts on both seasonal and spatial scales, which is a challenging task. A useful tool to achieve
80 such an integrated perspective is a high-resolution 3D coupled hydrodynamic-biogeochemical
81 model.

82 Disko Bay is located on the west coast of Greenland (Fig. 1) near the southern border of the
83 maximum annual Arctic sea ice extent, and is influenced by both sub-Arctic waters from
84 southwestern Greenland and Arctic waters within the Baffin Bay (Gladish et al., 2015; Rysgaard
85 et al., 2020). The bay has a pronounced seasonality in sea ice cover (Møller and Nielsen, 2020).
86 Over the last 40 years, there has been a pronounced decrease in sea ice cover, and also the year-
87 to-year variations have increased in the last decade (Fig 2, Hansen et al., 2006, the Greenland
88 Ecosystem monitoring program, <http://data.g-e-m.dk>). For the primary producers particularly the
89 decrease in sea ice cover during the time of the spring bloom in April is important (Møller and
90 Nielsen, 2020). In addition to the seasonal sea ice cover changes, the bay also experiences large
91 seasonal changes in freshwater input from the Greenland ice sheet, particularly during the
92 summer months (Fig. 2, 3). The large marine terminating glacier Sermeq Kujalleq (Jakobshavn
93 Isbræ) is found in the inner part of the bay. It is estimated that about 10% of the icebergs from
94 the Greenland ice sheet originate from this glacier (Mankoff et al., 2020a). Since the 1980s,
95 freshwater discharge from the Greenland Ice sheet to Disko Bay has almost doubled (Fig. 2,
96 (Mankoff et al., 2020b, 2020a). How these significant changes in sea ice dynamics and run-off

97 will impact the ecosystem in Disko Bay, one of the most important areas for biodiversity and
98 fisheries around Greenland (Christensen et al. 2012), is still not well understood.

99 In this study, we investigate the combined effect of changes in sea ice cover and the Greenland
100 ice sheet freshwater discharge on the phenology/seasonal timing and annual magnitude and
101 spatial distribution of the phytoplankton production in Disko Bay. We do so using a high-
102 resolution 3D coupled hydrodynamic-biogeochemical model validated against in situ
103 measurement of salinity, temperature, nutrients, phytoplankton, and zooplankton biomass. The
104 validated model allows us to estimate the impact of sea ice cover and freshwater discharge on
105 productivity with a higher temporal and spatial resolution than would be possible from
106 measurements alone.

107 2 Methods

108 2.1 Hydrodynamic model

109 The model was set up using the FlexSem model system (Larsen et al. 2020). FlexSem is an open
110 source modular framework for 3D unstructured marine modelling. The system contains modules
111 for hydrostatic and non-hydrostatic hydrodynamics, 3D pelagic and 3D benthic models, sediment
112 transport and agent-based models. The FlexSem source code and precompiled source code for
113 Windows (GNU General Public License) can be downloaded at
114 <https://marweb.bios.au.dk/Flexsem>. The specific code for the Disko set-up can be downloaded
115 on Zenodo.org (Larsen, 2022; Maar et al., 2022).

116 Bathymetry were obtained from the 150x150 m resolved IceBridge BedMachine Greenland,
117 Version 3 (<https://nsidc.org/data/IDBMG4> (Morlighem et al., 2017)) and interpolated to the
118 FlexSem computational mesh using linear interpolation. The 96,300 km² large computational
119 mesh for the Disko Bay area was constructed using the mesh generator JigSaw
120 (<https://github.com/dengwirda/jigsaw>) (Fig. 1). It consists of 6349 elements and 34 depth z-
121 layers with a total of 105678 computational cells. The horizontal resolution varies from 1.8 km
122 in the Disko Bay proper, 4.7 km in Strait of Vaigat and 16 km towards the semi-circular Baffin
123 Bay open boundary. In the deepest layers, the vertical resolution is 50 m, decreasing towards the
124 surface, where the top 5 layers are 3.5, 1.5, 2.0, 2.0 and 2.0 meters thick, respectively. The

125 surface layer thickness is flexible allowing changes in water level e.g., due to tidal elevations.
126 The model time step is 300 seconds and has been run for the period from 2004 to 2018.

127 **2.2 Biogeochemical model**

128 The biogeochemical model in the FlexSem framework was based on a modification of the
129 ERGOM model that originally was applied to the Baltic Sea and the North Sea (Maar et al.,
130 2011, 2016; Neumann, 2000) (Appendix A). In the Disko Bay version, 11 state variables
131 describe concentrations of four dissolved nutrients (NO_3 , NH_4 , PO_4 , SiO_2), two functional groups
132 of phytoplankton (diatoms, flagellates), micro- and mesozooplankton, detritus (NP), detritus-
133 silicon, and oxygen. Cyanobacteria present in the Baltic Sea version of the model are removed in
134 the current set-up, because cyanobacteria are of little importance in high-saline Arctic waters
135 (Lovejoy et al., 2007). Further, pelagic detrital silicon was added to better describe the cycling
136 and settling of Si in deep waters. The model currency is N using Redfield ratios to convert to P
137 and Si. Chlorophyll *a* (Chl *a*) was estimated as the sum of the two phytoplankton groups
138 multiplied by a factor of 1.7 mg-Chl/mmol-N (Thomas et al., 1992). The calanoid copepod *C.*
139 *finmarchicus* generally dominates the mesozooplankton biomass (Møller and Nielsen, 2020) and
140 the physiological processes were parameterized according to previous studies (Møller et al.,
141 2012, 2016). The model considers the processes of nutrient uptake, growth, grazing, egestion,
142 respiration, recycling, mortality, particle sinking and seasonal mesozooplankton migration in the
143 water column and overwintering in bottom waters. NPP was estimated as daily means of
144 phytoplankton growth after subtracting respiration and integrated over 30 m depth corresponding
145 to the productive layer. The timing of the seasonal *C. finmarchicus* migration was calibrated
146 against in situ measurements of their vertical distribution over time (Møller and Nielsen, 2019).
147 Light attenuation (*kd*) is a function of background attenuation (water turbidity, *kdb*) and
148 concentrations of detritus and Chl *a* (Maar et al., 2011). Turbidity is strongly correlated with
149 salinity and the background attenuation was described as a function of salinity: $kdb=0.80\text{-salinity}$
150 $\times 0.0288$ for salinity < 25 according to measurements across a salinity gradient in another
151 Greenland fjord, the Young Sound (Murray et al., 2015) and set to a constant of 0.08 m^{-1} for
152 salinity >25 according to monitoring data in the Disko Bay $69^\circ 14' \text{ N}$, $53^\circ 23' \text{ W}$ (data.g-e-m.dk,
153 <https://doi.org/10.17897/WH30-HT61>).

154 –Light optimum was changed for both phytoplankton groups during calibration to fit with the
155 timing of the spring bloom (Appendix A). Background mortality of microzooplankton was
156 increased to account for other grazing pressure than from *C. finmarchicus*.

157 **2.3 Freshwater and nutrient discharge**

158 We used the MAR and RACMO regional climate model (RCM) runoff field to compute
159 freshwater discharge. Ice runoff is defined as ice melt + condensation – evaporation + liquid
160 precipitation – refreezing. Land runoff is computed similarly, but there is no ice melt term
161 (although there is snow melt). Daily simulations of runoff were routed at stream scale to coastal
162 outlets, where it is then called ‘discharge’. Precipitation onto the ocean surface is not included in
163 the calculations (Mankoff et al., 2020a). Within Disko Bay, 235 streams discharge liquid water,
164 of which 97.5 % of the water comes from just 30 streams.

165 Fourteen points were selected within the model domain to represent the freshwater inflow. The
166 locations were manually selected to best represent the location of the largest rivers/inflows and
167 the spatial distribution of freshwater inflow in the model domain. The inflow from the 30 largest
168 rivers were manually aggregated into the 14 point sources by evaluating the geographical
169 location in relation to the coastal layout. This land run-off was inserted into the nearest model
170 cell in the surface layer. Although subglacial discharge enters at depth, it rises up the ice front
171 within a few 10s to 100s of meters of the ice front and within the grid cell at the ice boundary
172 (1800 -3200 m wide) will reach its neutral isopycnal here assumed to be the surface layer
173 (Mankoff et al., 2016). Thus, ice runoff ~~were~~was inserted in the surface layer. Solid ice discharge
174 was computed from ice velocity, ice thickness, and ice density at marine terminating glaciers
175 (Mankoff et al., 2020b). Within our modelling area in Disko Bay four glaciers discharge icebergs
176 into fjords, of which the majority comes from Sermeq Kujalleq (Jakobshavn Isbræ). Solid ice
177 was inserted where glaciers terminate directly into fjords (Fig. 1). At these four localities with
178 marine terminating glaciers, the freshwater contribution as solid ice was assumed to be equally
179 distributed in the top 100 m assuming that the majority of the solid ice are small pieces that melts
180 quickly as evidenced by the lack of brash ice generally seen in Disko Bay. Thus, we do not
181 consider the large icebergs calved by Sermeq Kujalleq and their input of freshwater along the
182 route in the bay. Land discharge of nitrate, phosphate, and silicate at the 14 point sources was

183 assumed to be constant in time with concentrations of 1.25, 0.20 and 10.88 mmol m⁻³,
184 respectively (Hopwood et al., 2020).

185 **2.4 Hydrodynamic open boundary and initial data**

186 At the semi-circular open boundary towards the Baffin Bay, the model was forced with ocean
187 velocities, water level, salinity, and temperature obtained from a coupled ocean- and sea ice
188 model (Madsen et al., 2016) provided by the Danish Meteorological Institute (DMI). The DMI
189 model system consists of the HYbrid Coordinate Ocean Model (HYCOM, e.g., Chassignet et al.,
190 2007) and the Community Ice Code (CICE, (Hunke, 2001; Hunke and Dukowicz, 1997) coupled
191 with the Earth System modeling Framework (ESMF) coupler (Collins et al., 2005). The
192 HYCOM-CICE set-up at DMI covers the Arctic Ocean and the Atlantic Ocean, north of about
193 20°S, with a horizontal resolution of about 10 km. Further details on the HYCOM-CICE model
194 system can be found in Appendix B.

195 The 2D (water level) and 3D parameters were interpolated to match the open boundary in the
196 FlexSem Model setup using linear interpolation. Correspondingly, initial fields of temperature,
197 salinity and water level were interpolated from the HYCOM-CICE model output.

198 **2.5 Observed sea ice cover**

199 The long term sea ice cover within Disko Bay was extracted from the sea ice concentration data
200 provided by the EUMETSAT Ocean and Sea Ice Satellite Application Facility (OSISAF,
201 www.osi-saf.org, Lavergne et al., 2019) on a daily basis (AICE). The Disko Bay area is here
202 defined as longitude and latitude range between 54.0°W and 51.5°W and 68.7°N to 69.5°N
203 respectively. As the OSISAF product is seasonally quite noisy for low sea ice concentrations, we
204 made a cutoff at 40 percent before we take the mean for the entire area. The exact cut-off value
205 does not matter much on the resulting time series, as the freeze-up and melt-down period is quite
206 fast for the area. Furthermore, we obtained sea ice observations from the Greenland Ecosystem
207 Monitoring (GEM) program (<http://data.g-e-m.dk>, <https://doi.org/10.17897/SVR0-1574>) in
208 which ice coverage is registered daily by visual inspection from the laboratory building at
209 Copenhagen University's Arctic station in Qeqertarsuaq.

210 **2.6 Surface forcing data**

211 At the surface, the model was forced by sea ice concentration, wind drag and heat fluxes. The ice
212 cover percentage modifies the wind drag, heat balance and light penetration in the model. [Glacier](#)
213 [ice cover was assumed to be present throughout the year in the Jakobshavn Isbræ near Ilulissat](#)
214 [with the ice edge located at the mouth of the fjord whereas land- and ice runoff were located at](#)
215 [the sub-arms of the fjord \(Figure 1\)](#). The surface heat budget model estimating the heat flux
216 (long- and short-wave radiation) was forced by wind, 2 meter atmospheric temperature, cloud
217 cover, specific humidity and ice cover. Photosynthetically active radiation (PAR) was estimated
218 from the short-wave radiation assuming 43% to be available for photosynthesis (Zhang et al.,
219 2010). The atmospheric forcing was provided by DMI from the HIRLAM (Yang et al., 2005)
220 and HARMONIE (Yang et al., 2017; 2018) meteorological models using the configuration with
221 the best resolution available for our simulation period. The resolution was 15 km until May
222 2005, then increased to about 5 km until March 2017, and since then to 2.5 km. Ice cover was
223 obtained from the HYCOM-CICE model output.

224 **2.7 Biogeochemical open boundary and initial data**

225 Initial data and open boundary conditions for ecological variables were obtained from the pan-
226 Arctic 'A20' model at NIVA Norway. This was based on a 20 km-resolution ROMS ocean-sea
227 ice model (Shchepetkin and McWilliams, 2005, Roed et al., 2014) coupled to the ERSEM
228 biogeochemical model (Butenschön et al., 2016), run in hindcast mode and bias-corrected
229 towards a compilation of in situ observations (Palmer et al., 2019). This model provided bias-
230 corrected output for (nitrate, phosphate, silicate, dissolved oxygen) plus raw hindcast output for
231 ammonium, detritus (small, medium and large fractions), 6 groups of phytoplankton and 3
232 zooplankton groups. The picophytoplankton, Synechococcus, nano-, micro-phytoplankton and
233 prymnesiophyte biomasses from ERSEM were summed to provide data for the autotrophic
234 flagellate group in ERSEM, while the diatom functional group was the same in both models.
235 The detritus pool in ERSEM was the sum of the three detritus size fractions in ERSEM. The
236 A20 data were provided as weekly means on a 20 km grid and linearly interpolated to the
237 FlexSem grid. ERSEM provided data through 2014, then 2014 was repeated for the following
238 years.

239 2.8 Validation

240 For model calibration and validation of the seasonality, we used reported research observations
241 of temperature, salinity, nutrients (nitrate, silicate, phosphate), Chl *a* concentrations and
242 mesozooplankton biomass collected during short-term field campaigns at the Disko Bay station
243 69° 14' N, 53° 23' W from 2004 to 2012 (e.g.(Møller and Nielsen, 2019)). Furthermore, we used
244 observations of the same variables from the same station provided by the Greenland Ecological
245 Monitoring (GEM) program running since 2016 in the Disko Bay (data.g-e-m.dk). However, the
246 data coverage is highly sporadic between years and months, and we therefore created a monthly
247 climatology (2004-2018) for the best-sampled depth layer 0-20 m (Møller et al, 2022). This
248 climatology was compared with monthly means extracted from the model at the same location
249 and depth range where 2004 was used for model calibration and means from 2005 to 2018 for
250 model validation. Mesozooplankton biomass in the model was assumed to mainly represent the
251 copepods *Calanus* spp. and for the conversion from N to carbon (C) biomass, we used 12 g-C
252 mol⁻¹ and C:N= 6.0 mol-C mol-N⁻¹ (Swailethorp et al., 2011).

253 Additionally, the model was validated spatially using remote sensing (RS) data of sea surface
254 temperature (SST) and Chl *a* concentrations for spring (April to June) and summer (July to
255 September) for 2010 and 2017. RS data was obtained from the Copernicus Marine Service (ref
256 <https://marine.copernicus.eu>). For SST we used the L4 product
257 'SEAICE_ARC_PHY_CLIMATE_L4_MY_011_016-TDS', which has spatial resolution of 0.05
258 degree and daily time resolution. For Chl *a* we used the data service
259 'OCEANCOLOUR_ARC_CHL_L4_REP_OBSERVATIONS_009_088-TDS' (L4 product
260 based on the OC5CCI algorithm), which has a spatial resolution of 0.01 degree and monthly time
261 resolution. Chl *a* concentrations were log-transformed because they span several orders of
262 magnitude. For both SST and Chl *a* comparisons, the RS data were interpolated to cell center
263 points of the horizontal FlexSem grid using a bi-linear scheme. Validation was only performed at
264 spatial points, where RS data has at least one quality-accepted data entry (i.e. sufficient visibility
265 without ice and cloud cover) for the respective validation periods.

266 The model skill was assessed by different metrics. The Pearson correlation between observations
267 and model results was estimated for the seasonal data and spatial data assuming a significance
268 threshold of $p < 0.05$. The other metrics were:

269 Mean Error (ME) is the mean of the differences between observations x and model results y :

$$270 \quad ME = \frac{1}{N} \sum_{i=1}^N (y_i - x_i)$$

271 where N is the total number of data points. The Root Mean Square Error (RMSE) is the square
272 root of the mean squared error between x and y :

$$273 \quad RMSE = \sqrt{\frac{1}{N} \sum_{i=1}^N (y_i - x_i)^2}$$

274 The average cost function (cf) is defined as (Radach and Moll 2006):

$$275 \quad cf = \frac{1}{N} \sum_{i=1}^N \frac{|(y_i - x_i)|}{SD(x)}$$

276 Depending on the cf number, it is possible to assess the performance of the model as “very good”
277 (<1), “good” (1-2), “reasonable” (2-3), and “poor” (>3).

278 Microzooplankton data was available from the literature for 1996/97 (Levinsen and Nielsen,
279 2002) and April-May 2011 (Menden-Deuer et al., 2018). Thus, it was not possible to create a
280 climatology, but the available data was used for visual comparison with model data. Data from
281 Levinsen and Nielsen (2002) was depth integrated (g-C m^{-2}), and converted to mg-C m^{-3} by
282 assuming that the total biomass was distributed uniformly over the upper 25 m (Levinsen et al.,
283 2000). Data from Menden-Deuer (2018) was from fluorescence maximum, and this was assumed
284 to represent the upper 20 m. The conversion from nitrogen to carbon biomass was obtained from
285 the Redfield ratio= $6.625 \text{ mol-C mol-N}^{-1}$ and the mol weight of 12 g-C mol^{-1} .

286 **2.9 The impact of sea ice cover and discharge on primary productivity**

287 An overall indication of the relationship between NPP and sea ice cover and freshwater
288 discharge was obtained by Pearson product moment correlation analysis between annual
289 estimates of these for the entire Bay, as defined by the box in figure 1. We further evaluated the
290 impact of sea ice cover and freshwater discharge on the NPP on a spatial scale. To do this we
291 perform correlation analysis between the annual NPP and the average sea ice cover March-April
292 in each model grid cell for 2004-2018. To evaluate the impact of the discharge we performed
293 similar correlations with average annual surface salinity instead of sea ice cover. The

294 assumption behind the choice is that the surface salinity scales with the impact of freshwater
295 discharge.

296 To demonstrate the effect of sea ice cover and distance to the glacial outlet on the temporal
297 development of nitrogen concentration, Chl *a*, and NPP, two stations and two years with
298 different features were selected. The first station was located in the open bay and the other
299 station close to the Ilulissat Isfjord (Bay and Glacier station, Fig. 1). The two years 2010 and
300 2017 were chosen according to differences in both irradiance and sea ice cover, one (2010) with
301 low sea ice cover and high irradiance and the other (2017) with high sea ice cover and low
302 irradiance.

303 To further evaluate the impact of sea ice cover and freshwater discharge we performed some
304 simple “extreme” model scenarios (Table 1). We tested the potential effect on primary
305 productivity in 2010 (low sea ice cover) and 2017 (high sea ice cover) in scenarios with no sea
306 ice, no freshwater discharge or 2 times the reference discharge, as well as the combinations, by
307 changing the model forcing accordingly.

308 We furthermore for 2010 tested the impact of inserting the ice runoff at the glacier grounding
309 line instead of the surface layer where glaciers terminate directly into fjords (Fig. 1).

310 3 Results

311 3.1 Freshwater discharge and sea ice cover

312 50 years ago, the average annual liquid runoff from the ice sheet to the study area was generally
313 $\sim 1000 \text{ m}^3 \text{ s}^{-1}$ ($913 \pm 2214 \text{ SD m}^3 \text{ s}^{-1}$, 1958-1969), whereas during the last 20 years is has varied
314 between 2000 and $4500 \text{ m}^3 \text{ s}^{-1}$ ($2591 \pm 724 \text{ SD m}^3 \text{ s}^{-1}$, 2000-2019) (Fig. 2). The precipitation
315 over land has also increased from about 200 ($197 \pm 40 \text{ SD m}^3 \text{ s}^{-1}$) to $400\text{-}500 \text{ m}^3 \text{ s}^{-1}$ ($469 \pm 77 \text{ SD}$
316 $\text{m}^3 \text{ s}^{-1}$). The calving of solid ice from the glaciers has only been estimated for the last 30 years,
317 but it also shows an increasing trend although since the maximum in 2013, the production of ice
318 has been lower (Fig. 2). Thus, for all three sources of freshwater the overall long-term trend is an
319 increase, but for the model period between 2004 and 2018 no trend was evident (Fig. 3e). The
320 freshwater discharge from solid ice was relatively constant across the year, whereas the liquid
321 contribution peaked during summer, from June to August, and drops to almost zero in the winter
322 (Fig. 3f).

323 The sea ice cover in Disko Bay has generally decreased during the last 35 years (Fig. 2).
324 However, the last 15 years have been characterized by large interannual variation with some
325 years with virtually no ice and others with sea ice cover as in the 1990s. During the model period
326 the ice generally did not form before late December, and the maximum ice cover was seen in
327 March (Fig. 3)

328 **3.2 Validation of the model**

329 The seasonal timing and general level of temperature, salinity, nutrients, Chl *a* and
330 mesozooplankton agreed well with the data climatology from the field sampling south of Disko
331 Island (Fig. 4, Table 2). All correlations between observational and model data were significant
332 ($R > 0.82$). The model performance assessed by the average cost function *cf* was “very good” for
333 all parameters. Modelled Chl *a* showed highest interannual variability in spring and the
334 chlorophyll bloom was somewhat too weak (~30% less), and the winter silicate too high, relative
335 to the climatological mean observations.

336 The spatial distribution patterns of Chl *a* and temperature at the surface were compared to
337 satellite estimates for the two years 2010 and 2017 used in the scenarios representing low and
338 high sea ice cover, respectively (Table 3, Fig. C1). The correlations were significant for all
339 relations ($p < 0.01$), and the *cf* number was “very good” or “good” for all (Table 3). Surface
340 temperature tended to be higher in spring and lower in summer in the model compared to the
341 satellite estimates. Chl *a* concentrations were generally higher in the model than in the satellite
342 data, especially in spring 2017 (Fig. C1).

343 **3.3 Seasonal and spatial patterns of NPP in Disko Bay**

344 Primary production starts as sea ice cover decreases and irradiance increases in February (Fig. 3).
345 Extensive sea cover may reduce light availability in the water column and thereby limit
346 production, and the interannual variation in NPP is highest in April because of the variation in
347 sea ice cover, causing light availability in the water to vary accordingly. Highest NPP was in
348 May and June with about $800 \text{ mg-C m}^{-3} \text{ d}^{-1}$ when light influx was highest and sea ice was
349 entirely melted (Fig. 3).

350 The impact of sea ice is illustrated by comparing a year with low (2010) and high (2017) sea ice
351 cover, where the spring bloom is about 25-30 days earlier in 2010 than in 2017 (Fig. 5).

352 Comparing a station close to and far from the glacier illustrates the potential impact of the
353 freshwater peak in late summer, as NPP is 2-3 times higher during this period at the station close
354 to the glacier (Fig. 5).

355 Concerning the spatial distribution in the spring period (March to June), high NPP was seen
356 across the bay, with the lowest values found southeast of the Disko Island and southwest of the
357 Bay following the bathymetry. In the later summer period (July to October), primary production
358 was more confined to the coast (Fig. 6).

359 **3.4 Annual variability of NPP**

360 The annual average NPP in the Bay estimated from the model varied between 90 and 147 g-C
361 m⁻² year⁻¹ with an average of 129±16 (SD) (Fig. 3). Generally, years with high sea ice cover in
362 spring had lower average annual NPP (Fig. 3, Pearson product moment correlation coefficient r
363 = -0.63, $p=0.01$), while higher discharge was associated with higher annual primary productivity
364 (Fig. 3, $r = 0.51$, $p=0.05$).

365 To evaluate the spatial dependency, we performed an analysis of the correlation between the sea
366 ice cover in March to April and the annual NPP in each model grid cell. This showed a negative
367 relationship widespread in the model domain, i.e. the more sea ice, the lower NPP (Fig. 7). One
368 exception was in the south part of the model domain, where the correlation was positive. The
369 impact of the freshwater discharge on the NPP was generally positive in areas up to ~50 km from
370 the discharge and additionally in the northern part of Disko Bay, as reflected by the negative
371 correlation to surface salinity in these areas (Fig. 7).

372 **3.5 Model scenarios with sea ice cover and discharge**

373 We studied some simple model scenarios where sea ice cover was assumed to be zero and the
374 discharge was either doubled or cut off, with basis in 2010 and 2017, which had low and high sea
375 ice cover, respectively, and opposite discharge (Fig. 3). These scenarios underline the
376 complexity of the dynamics of the system, with some areas experiencing increased NPP while
377 others experience a decrease (Figs. 8, 9). Furthermore, it allows us to evaluate the impact of the
378 uncertainty of actual freshwater runoff. The year 2017 had relatively high and late ice cover (Fig.
379 3) and applying a scenario of no ice leads to an increase in bay-scale annual NPP of 34 %,
380 although spatial variability is high and annual NPP changes vary between -20% and 98% (Fig.

381 9). For 2010, a year that already had low sea ice cover, the same scenario led to minor changes in
382 the annual NPP on bay scale (2 %, Fig. 8). For both years, the omission of freshwater discharge
383 generally led to a decrease in annual NPP; this effect was small on the bay scale (-2 to 0%), but
384 reached -64% in near-coastal areas under glacial/runoff influence. Similarly, the effect of
385 doubling of the discharge was minor on the bay scale (0-1%), but reached up to 55 and 68 %
386 NPP increase in runoff-influenced areas in 2010 and 2017, respectively. The effects of sea ice
387 and freshwater discharge changes combined in an approximately additive manner (Figs. 8, 9).
388 When the forcing from sea ice cover and freshwater discharge were set to be zero in 2010 and
389 2017, NPP in 2017 was were still 20% smaller than the 2010. This illustrates the importance of
390 other factors for NPP like wind, cloud cover and inflow to the bay.

391 When the Horizontal (East-West) current velocity profiles at the ice edge (water depth of 241 m)
392 of Jakobshavn Isbræ showed an outgoing westly direction with highest outflow at 150-200 m
393 depth from March to October (Figure C4a). Vertical velocities showed an upward transport with
394 highest values close to the bottom at 190-216 m depth (Figure C4b). The scenario with no runoff
395 (noQNP) showed weaker horizontal transports and less upwelling at the ice edge (Figure C4).
396 When ice run-off was inserted/released at the glacier grounding line instead of at the surface layer
397 as in the standard model runs, only a small increase of horizontal and vertical velocities was
398 found at 90-200 m depth relative to the baseline. In addition, a small spatial displacement of the
399 primary production was seen (Fig C4C5). The stratification and vertical distribution of nutrients,
400 Chl *a* and primary production were not changing much, just establishing a bit further offshore in
401 the late summer months (Fig C3+C5C6). The effect on the bay primary productivity is only
402 minor (<1%).

403 4 Discussion

404 Primary productivity is an essential ecosystem service that shapes the structure of the marine
405 ecosystem and fuels higher trophic levels such as fish that is vital for the Greenlandic society. It
406 is therefore important to estimate potential outcomes for primary production under the continued
407 warming and subsequent ice melt. For the coastal ocean, especially around Greenland, it is
408 imperative to quantify how changes in sea ice cover and run-off combine to determine the
409 availability of the two key resources, light and nitrate, determining the magnitude and phenology
410 of primary production. Sea ice cover and run-off influence light and nitrate availability through

411 several intermediate processes, and their peak impact often occurs in different areas and in
412 different months. The spatial-temporal variability and complexity of processes involved requires
413 an approach where detailed *in situ* observations are combined with remote sensing and
414 modelling. The present study is to our knowledge the first attempt to apply this approach for
415 coastal Greenland.

416 Our model results show that reduction in spring sea ice cover changes the plankton phenology
417 but also increases the magnitude of annual production in Disko Bay. This suggests that there is a
418 replenishment of nitrate into the photic zone to sustain the continued productivity beyond the
419 initial depletion following the spring bloom. Part of the nitrate input is coupled to the run-off, but
420 the high modelled productivity from April to July, when liquid run-off is limited suggest that
421 vertical mixing fueled by wind and tide is important. That less sea ice cover will lead to
422 increased NPP is in agreement with other studies from the open Arctic areas (Arrigo and van
423 Dijken, 2015; Vernet et al., 2021). In other Greenland fjords, the turbulence driving vertical
424 mixing has been shown to be very low (Bendtsen et al., 2021; Randelhoff et al., 2020), but is
425 seems likely that the open Disko Bay with a tidal amplitude of up to 3 m (Thyrring et al., 2021)
426 could have an efficient vertical flux of nitrate into the photic zone.

427 Our study site was chosen because the Disko Bay in mid-west Greenland is considered a hot-spot
428 for marine biodiversity and fisheries, and because it is an area where both sea ice cover and
429 glacial run-off are likely to be important for productivity. But regional variability is high across
430 the coastal ocean around Greenland. For example, ice cover is very limited in most of SW
431 Greenland and is unlikely to drive changes in future primary production, whereas glacial run-off
432 is less in NE Greenland compared to the rest of Greenland. Furthermore, the dominance of land
433 or marine terminating glaciers as in Disko Bay will be important for the outcome of increased
434 glacial run-off on individual fjord scale (Hopwood et al., 2020; Lydersen et al., 2014). Finally,
435 winter concentration of nitrate and vertical gradients in summer differ between the East and West
436 coast, with low nitrate content in the East Greenland Current generally causing lower
437 productivity compared to West Greenland (Vernet et al. 2021).

438 **4.1 Phenology of primary producers**

439 A main advantage of the model is that it allows us to estimate the productivity with a higher
440 temporal and spatial resolution than would be possible from measurements alone. The sea ice

441 cover had a clear effect on the spring NPP. When sea ice cover is low, spring NPP is starting
442 earlier compared to years with high sea ice cover, and the largest variation in NPP between years
443 is seen in the spring months (Fig. 3). The performed scenarios support the importance of sea ice
444 cover, i.e. the absence of sea ice leads to a considerable increase in the annual NPP on bay scale
445 (Fig. 9). Potentially, NPP could start as early as February if considering the light availability.
446 However, for NPP to increase would also require the water column to stabilize, i.e. wind mixing
447 would need to be sufficiently low (Tremblay et al., 2015). In contrast, the timing of the formation
448 of the sea ice in fall is not important for the primary productivity, since the sea ice in Disko Bay
449 does not form before the light has largely disappeared. This is in contrast to high Arctic systems
450 where sea ice normally forms earlier and a delay in the formation of sea ice in fall may result in
451 autumn blooms (Ardyna et al., 2014).

452 **4.2 Spatial distribution of NPP**

453 In our analysis, we see a positive effect of the freshwater discharge on the primary productivity
454 locally and during the summer months. This effect is related to the upwelling that is enhanced by
455 the freshwater discharge (Fig. C2, C3). The nutrient concentration in the discharge (1.25 μM ,
456 Hopwood et al., 2020) is lower than the average concentration in the upper 30 m during summer
457 at the station near the glacier (e.g. $\sim 4 \mu\text{M NO}_3$) (Fig. 7), and will therefore not lead to increased
458 NPP. This is in accordance with the general picture from glacial affected environments. River
459 discharge may on the other hand carry higher nutrient concentrations, particularly of nitrogen
460 (Hopwood et al., 2019).

461 We used two approaches to evaluate the spatial scale of the effect freshwater discharge. The
462 correlation analyses using salinity as a proxy for the discharge (Fig. 7) suggest that the discharge
463 may influence ~ 50 km away from the source. The scenarios where we alter the discharge
464 suggest that the effect is only a couple of percent considering NPP on the Bay scale, whereas on
465 a more local scale near the glacier the importance is higher (-64% to 147%, Fig. 8 and 9).

466 Godthåbsfjord- is situated further south at the west coast of Greenland and is fjord system less
467 directly affected by the ocean dynamics than the open Disko Bay. Here glacial runoff has been
468 suggested to affect the seasonal development of phytoplankton 120 km away from the glacier
469 (Juul-Pedersen et al., 2015). Furthermore, it was found that 1-11% of the NPP in the Fjord
470 systems is supported by entrainment of N by the three marine terminating glaciers (Meire et al.,

471 2017). Considering only the parts of the fjord directly impacted by the discharge the estimate
472 were 3 times higher (Hopwood et al., 2020).Analyses from Svalbard fjords impacted by glacial
473 discharge showed positive spatiotemporal associations of Chl *a* with glacier runoff for 7 out of
474 14 primary hydrological regions but only within 10 km distance from the shore (Dunse et al.,
475 2022).

476 The modelling in this study allows us to evaluate the combined effect of changes in sea cover
477 and freshwater discharge in the coastal ecosystem of the Disko Bay. Importantly, this study also
478 illustrates that within the Arctic coastal zone, the combination of different climate change effects
479 may lead to different responses within relatively small distances. Thus, while we can suggest a
480 general increasing trend in the NPP, this may not be evident when considering local
481 observations. This is important to consider when planning and evaluating field investigations.

482 **4.3 Modelled NPP versus other estimates**

483 The biogeochemical model was validated using all available observations. These are all
484 concentrations (nutrients) or standing stocks (phytoplankton, zooplankton). The satisfactory
485 validation is an indication that the rates are also adequately described. Still, it is desirable also to
486 have direct comparison with rate measurements. There are no available NPP measurements for
487 our modelling period. However, data are available from 1973-1975 (Andersen, 1981) and
488 1996/97 (Levinsen and Nielsen, 2002) and 2003 (Sejr et al., 2007). The data from 1996/97 were
489 *in situ* bottle incubations in the upper 30 m, and no further information on methodology was
490 given (referred to as unpublished). The sea ice cover was generally high in Disko Bay at that
491 time (Fig. 4) and we therefore compare the seasonal development to our model estimates from
492 2017, a year with extensive sea ice cover. The estimate of the annual production from 1996/97
493 was 28 gC m⁻² d⁻¹ less than half the estimate from 1970s of 70 gC m⁻² d⁻¹, and the modeling
494 estimates from 2017 of 82 gC m⁻² d⁻¹ at the same station. The measurements do, however, both
495 agree with the model on the seasonal timing of NPP with an increase in NPP between March and
496 April, and the Pearson correlation coefficients between measurements and model results were
497 0.84, p<0.001 (1996/7) and 0.69, p<0.05 (1973-75). Data from 2003 (Sejr et al., 2007) are from a
498 shallow cove only in two shorter periods, but the production of 195 mgC m⁻² d⁻¹ in April aligns
499 well with our estimates, whereas the value in September 27 mgC m⁻² d⁻¹ is somewhat lower.

Formatted: Danish

Field Code Changed

Formatted: Danish

Field Code Changed

Formatted: Danish

Formatted: Danish

500 Average estimates of NPP from Arctic glacial fjords with marine terminating glaciers are
501 reported to be 400-800 mg-C m⁻² d⁻¹ during July to September (Hopwood et al., 2020). In the
502 Arctic Ocean, shelf regions estimates from satellite observations are 400-1400 mgC m⁻² d⁻¹ in
503 April to September during 1998 to 2006 (Pabi et al., 2008). Thus, overall, our model estimates of
504 NPP in Disko Bay of 378-815 mgC m⁻² d⁻¹ between April and September (Fig. 3) are in the same
505 range as other estimates.

506 In another modelling study, a physically-biologically coupled, regional 3D ocean model
507 (SINMOD) was compared with ocean color remote sensing (OCRS). Both OCRS and SINMOD
508 provided similar estimates of the timing and rates of productivity in of the shelves around
509 Greenland (Vernet et al., 2021). In the region including Disko Bay, the modelled NPP was
510 generally suggested to be much lower (20-23 gC m⁻² yr⁻¹) than our estimate (90-147 gC m⁻² yr⁻¹)
511 and the bloom was suggested to generally start later (late May). However, their model mainly
512 covered the shelf area north of Disko Bay and did not resolve the plume outside the ice fjord.
513 Moreover, the estimates from OCRS (50 gC m⁻² yr⁻¹) were about double the modelled values,
514 and furthermore could only be recorded after ice break-up when the bloom was already on its
515 maximum (Vernet et al., 2021), suggesting that it could be much higher.

516 **4.4 Uncertainty and potential model improvement**

517 We model the impact of turbidity on light conditions in the water column as a simple relationship
518 between salinity and light attenuation. More sophisticated light models may be applied in future
519 models (Murray et al., 2015). However, in a relatively open water system like Disko Bay, the
520 effect of increased light attenuation due to increased turbidity is only expected within 5-10
521 kilometers of the glacial outlet. Moreover, we do not expect an impact on the total NPP in the
522 bay since the nutrients will anyway be used within the bay. A comparison between the spatial
523 distribution of surface Chl *a* assessed by satellite and the model showed a significant correlation
524 and the model performance were evaluated good to excellent (Table 3). Still, visual inspections
525 of the two maps suggest that the effect of the discharge on the Chl *a* spatial distribution were
526 more local and concentrated in the model than what is suggested by the satellite estimates (Fig.
527 C1). Thus, a higher precision in the spatial distribution of the phytoplankton may be achieved by
528 improving the model parametrization of light attenuation, e.g. by inserting a passive tracer
529 reflecting the turbidity in melt water. A more dynamic description of acclimation of primary

530 productivity to different light under nutrient conditions (Ross and Geider, 2009), may be
531 achieved by implementing variable element ratios (e.g., C:N) of phytoplankton instead of the
532 fixed ratios in the current model. The uncertainty in the different freshwater discharge source
533 may impact our estimates of marine productivity differently. Liquid runoff uncertainty and errors
534 are more likely to be random than bias, and when averaged together (over large spatial areas or
535 times) the uncertainty is reduced (Mankoff et al., 2020b). Conversely, solid ice discharge
536 uncertainty comes primarily from unknown ice thickness, which is time-invariant and therefore
537 must be treated as a bias term (Mankoff et al., 2020a). It does not reduce when averaged in space
538 or time.

539 -We do not specifically model the subglacial discharge of freshwater from the marine terminating
540 glaciers or from [melting of](#) the numerous large icebergs in the bay. Instead, the freshwater
541 discharge from solid ice was distributed equally across the upper 100 m in the locations where
542 marine terminating glaciers were present. Subglacial discharge that enters at depth, will rise up
543 the ice front within a few 10s to 100s of meters of the ice front (Mankoff et al., 2016), which is
544 within the grid cell ~~at the ice boundary.~~ [In size of the model we](#). We therefor inserted ice
545 ~~runoff discharge~~ in the [model](#) surface layer. ~~We performed a test of the impact of instead~~
546 ~~inserting that was found to be fully mixed in the water column during transport towards the ice~~
547 ~~edge.~~ [At the discharge at ice edge of the eel Jakobshavn Isbræ, modelled velocity profiles](#)
548 [confirmed a bottom upwelling due to higher outgoing water transport](#) at the ~~depth~~ [bottom](#) of the
549 [grounding line at the glacier](#) (Figure C4a, b) in accordance with previous studies of marine
550 terminating glaciers ([Fig C4+C5](#)), which will lead to [Hopwood et al. 2020](#)). [In the scenario with](#)
551 [no runoff \(noQNP\), the rise of outgoing transport and vertical velocities at depths below 100m](#)
552 [was severely reduced confirming the subglacial importance of ice discharge further away from for](#)
553 [the glacier. The effect of this observed dynamic](#) (Hopwood et al. 2020). [When the discharge](#)
554 [instead was inserted at the grounding line of the marine terminating glaciers, there was a limited](#)
555 [increase in the vertical velocity marginal](#) (Figure C5b). [Similarly, there was only a slight](#)
556 displacement of the [phytoplankton](#) bloom ~~slightly to~~ further offshore ~~with only and~~ very limited
557 changes in the stratification and vertical distribution of nutrients, Chl *a* and NPP (Fig
558 [C4+C5+C6](#)). The effect of the primary productivity of the Bay was <1%.

559 To be able to resolve the small-scale mixing between sub-glacial discharge and ambient fjord
560 water in the plume directly in front of the glacier a higher model resolution will be needed. A
561 study from another Greenland fjord suggests efficient mixing near the glacial terminus, which
562 means that the freshwater fraction in the surface water near the glacial front is only 5-7%, which
563 indicates that the mixing ratio between sub-glacial discharge and fjord water is 1 liter of
564 meltwater to 13-16 liters of fjord water (Mortensen et al., 2020). The capacity of buoyancy
565 driven upwelling of subglacial discharge to supply nutrients to the photic zone depends on
566 several factors including the depth of the freshwater input and the density and nutrient content of
567 the ambient fjord water. Our approach to distribute the solid ice freshwater input in the upper
568 100 m and the ice runoff in the surface layer is a first attempt to simulate the average conditions
569 across the study area. We were able to reproduce the general pattern of upwelling (Fig C2+C3)
570 and spatial dynamics of productivity, but the magnitude could be ~~underestimated~~under- or
571 overestimated. Models of high spatial and process resolution are mainly developed to describe
572 the transports of heat and salt to glacial ice, in order to estimate the melt (Burchard et al., 2022).
573 If the focus is to describe the fine scale processes in front of the glacier, the development within
574 these models may in the future be implemented in ocean models.

575 **4.5 Conclusions**

576 Two important drivers of changes in the Arctic coastal ecosystems are sea ice cover and glacial
577 freshwater discharge. This modelling study estimates the response of the pelagic net primary
578 (NPP) production to changes in sea ice cover and freshwater run-off in Disko Bay, West
579 Greenland, from 2004 to 2018. The difference in annual production between the year with lowest
580 and highest annual NPP was 63%. Our analysis suggests that sea ice cover was the more
581 important of the two drivers of annual NPP through its effect on spring timing and annual
582 production. Freshwater discharge, on the other hand, had a strong impact on the summer NPP
583 near to the glacial outlet. Hence decreasing ice cover and more discharge can work
584 synergistically and increase productivity of the coastal ocean around Greenland.

585 **5 Author contribution**

586 EFM, MAM, MS conceptualized the study. MAM, JL, EFM was responsible for the FLEXSEM
587 development and validation, MHR for HYCOM-CICE, PW for the Arctic 'A20' model, KM for
588 MAR/ RACMO, and AC for the remote sensing data. MAM and EFM analyzed, synthesized and

589 visualized the data. EFM prepared the initial draft, and all authors contributed to review and
590 editing.

591 6 Competing interests

592 The authors declare that they have no conflict of interest.

593 7 Acknowledgements

594 This research has been supported by the Programme for Monitoring of the Greenland Ice Sheet
595 (PROMICE) and the European Union's Horizon 2020 research and innovation program
596 (INTAROS, grant no. 727890), and the Danish Environmental Protection Agency (MST-113
597 00095 and j-nr 2019 - 8443). MHR was funded by the Danish State through the National Centre
598 for Climate Research. PW was funded by the Joint Programming Initiative Healthy and
599 Productive Seas and Oceans (JPI Oceans) project CE2COAST and the EU Horizons 2020 project
600 FutureMARES, and used resources provided by the Norwegian Metacenter for Computational
601 Science and Storage Infrastructure (Notur/Norstore projects nn9490k, nn9630k, and ns9630k).
602 Data from the Greenland Ecosystem Monitoring Programme were provided by the Department
603 of Ecoscience, Aarhus University, Denmark, in collaboration with the Department of
604 Geosciences and Natural Resource Management, Copenhagen University, Denmark. The authors
605 are solely responsible for all results and conclusions presented, and they do not necessary reflect
606 the position of the Danish Ministry of the Environment or the Greenland Government.

607 **References**

- 608 Andersen, O. G. N.: The annual cycle of phytoplankton primary production and hydrography in
609 the Disko Bugt area, West Greenland., *Meddelelser om Gronland, Biosci.*, 6, 1981.
- 610 von Appen, W. J., Waite, A. M., Bergmann, M., Bienhold, C., Boebel, O., Bracher, A., Cisewski,
611 B., Hagemann, J., Hoppema, M., Iversen, M. H., Konrad, C., Krumpen, T., Lochthofen, N.,
612 Metfies, K., Niehoff, B., Nöthig, E. M., Purser, A., Salter, I., Schaber, M., Scholz, D., Soltwedel,
613 T., Torres-Valdes, S., Wekerle, C., Wenzhöfer, F., Wietz, M. and Boetius, A.: Sea-ice derived
614 meltwater stratification slows the biological carbon pump: results from continuous observations,
615 *Nat. Commun.*, 12(1), 1–16, doi:10.1038/s41467-021-26943-z, 2021.
- 616 Ardyna, M., Babin, M., Gosselin, M., Devred, E., Rainville, L. and Tremblay, J.-É.: Recent
617 Arctic Ocean sea ice loss triggers novel fall phytoplankton blooms, *Geophys. Res. Lett.*, 41(17),
618 6207–6212, doi:10.1002/2014GL061047, 2014.
- 619 Ardyna, M., Mundy, C. J., Mayot, N., Matthes, L. C., Oziel, L., Horvat, C., Leu, E., Assmy, P.,
620 Hill, V., Matrai, P. A., Gale, M., Melnikov, I. A. and Arrigo, K. R.: Under-Ice Phytoplankton
621 Blooms: Shedding Light on the “Invisible” Part of Arctic Primary Production, *Front. Mar. Sci.*,
622 7(November), 1–25, doi:10.3389/fmars.2020.608032, 2020.
- 623 Arrigo, K. R. and van Dijken, G. L.: Continued increases in Arctic Ocean primary production,
624 *Prog. Oceanogr.*, 136, 60–70, doi:10.1016/j.pocean.2015.05.002, 2015.
- 625 Bendtsen, J., Rysgaard, S., Carlson, D. F., Meire, L. and Sejr, M. K.: Vertical Mixing in
626 Stratified Fjords Near Tidewater Outlet Glaciers Along Northwest Greenland, *J. Geophys. Res.*
627 *Ocean.*, 126(8), 1–15, doi:10.1029/2020JC016898, 2021.
- 628 Bitz, C. M. and Lipscomb, W. H.: An energy-conserving thermodynamic model of sea ice, *J.*
629 *Geophys. Res. Ocean.*, 104(C7), 15669–15677, doi:10.1029/1999jc900100, 1999.
- 630 Butenschön, M., Clark, J., Aldridge, J. N., Icarus Allen, J., Artioli, Y., Blackford, J., Bruggeman,
631 J., Cazenave, P., Ciavatta, S., Kay, S., Lessin, G., Van Leeuwen, S., Van Der Molen, J., De
632 Mora, L., Polimene, L., Saille, S., Stephens, N. and Torres, R.: ERSEM 15.06: A generic model
633 for marine biogeochemistry and the ecosystem dynamics of the lower trophic levels, *Geosci.*
634 *Model Dev.*, 9(4), 1293–1339, doi:10.5194/gmd-9-1293-2016, 2016.

635 Chassignet, E. P., Hurlburt, H. E., Smedstad, O. M., Halliwell, G. R., Hogan, P. J., Wallcraft, A.
636 J., Baraille, R. and Bleck, R.: The HYCOM (HYbrid Coordinate Ocean Model) data assimilative
637 system, *J. Mar. Syst.*, 65(1-4 SPEC. ISS.), 60–83, doi:10.1016/j.jmarsys.2005.09.016, 2007.

638 Cohen, J., Zhang, X., Francis, J., Jung, T., Kwok, R., Overland, J., Ballinger, T. J., Bhatt, U. S.,
639 Chen, H. W., Coumou, D., Feldstein, S., Gu, H., Handorf, D., Henderson, G., Ionita, M.,
640 Kretschmer, M., Laliberte, F., Lee, S., Linderholm, H. W., Maslowski, W., Peings, Y., Pfeiffer,
641 K., Rigor, I., Semmler, T., Stroeve, J., Taylor, P. C., Vavrus, S., Vihma, T., Wang, S., Wendisch,
642 M., Wu, Y. and Yoon, J.: Divergent consensus on Arctic amplification influence on
643 midlatitude severe winter weather, *Nat. Clim. Chang.*, 10(1), 20–29, doi:10.1038/s41558-019-
644 0662-y, 2020.

645 Collins, N., Theurich, G., DeLuca, C., Suarez, M., Trayanov, A., Balaji, V., Li, P., Yang, W.,
646 Hill, C. and da Silva, A.: Design and implementation of components in the Earth System
647 Modeling Framework, *Int. J. High Perform. Comput. Appl.*, 19(3), 341–350,
648 doi:10.1177/1094342005056120, 2005.

649 Dai, A. and Trenberth, K. E.: Estimates of freshwater discharge from continents: Latitudinal and
650 seasonal variations, *J. Hydrometeorol.*, 3(6), 660–687, doi:10.1175/1525-
651 7541(2002)003<0660:EOFDFC>2.0.CO;2, 2002.

652 Dee, D. P., Uppala, S. M., Simmons, A. J., Berrisford, P., Poli, P., Kobayashi, S., Andrae, U.,
653 Balmaseda, M. A., Balsamo, G., Bauer, P., Bechtold, P., Beljaars, A. C. M., van de Berg, L.,
654 Bidlot, J., Bormann, N., Delsol, C., Dragani, R., Fuentes, M., Geer, A. J., Haimberger, L., Healy,
655 S. B., Hersbach, H., Hólm, E. V., Isaksen, I., Kållberg, P., Köhler, M., Matricardi, M., McNally,
656 A. P., Monge-Sanz, B. M., Morcrette, J. J., Park, B. K., Peubey, C., de Rosnay, P., Tavolato, C.,
657 Thépaut, J. N. and Vitart, F.: The ERA-Interim reanalysis: Configuration and performance of the
658 data assimilation system, *Q. J. R. Meteorol. Soc.*, 137(656), 553–597, doi:10.1002/qj.828, 2011.

659 Dunse, T., Dong, K., Aas, K. S. and Stige, L. C.: Regional-scale phytoplankton dynamics and
660 their association with glacier meltwater runoff in Svalbard, *Biogeosciences*, 19(2), 271–294,
661 doi:10.5194/bg-19-271-2022, 2022.

662 Egbert, G. D. and Erofeeva, S. Y.: Efficient inverse modeling of barotropic ocean tides, *J.*
663 *Atmos. Ocean. Technol.*, 19(2), 183–204, doi:10.1175/1520-

664 0426(2002)019<0183:EIMOBO>2.0.CO;2, 2002.

665 Gladish, C. V., Holland, D. M. and Lee, C. M.: Oceanic Boundary Conditions for Jakobshavn
666 Glacier. Part II: Provenance and Sources of Variability of Disko Bay and Ilulissat Icefjord
667 Waters, 1990-- 2011, *J. Phys. Oceanogr.*, 45(2003), 33–63, doi:10.1175/JPO-D-14-0045.1, 2015.

668 Hansen, B. U., Elberling, B., Humlum, O. and Nielsen, N.: Meteorological trends (1991–2004) at
669 Arctic Station, Central West Greenland (69°15'N) in a 130 years perspective, *Geogr. Tidsskr. J.*
670 *Geogr.*, 106(1), 45–55, doi:10.1080/00167223.2006.10649544, 2006.

671 Hernes, P. J., Tank, S. E., Sejr, M. K. and Glud, R. N.: Element cycling and aquatic function in a
672 changing Arctic, *Limnol. Oceanogr.*, 66(S1), S1–S16, doi:10.1002/lno.11717, 2021.

673 Hibler, W. D.: A Dynamic Thermodynamic Sea Ice Model, *J. Phys. Oceanogr.*, 9(4),
674 doi:10.1175/1520-0485(1979)009<0815:adtsim>2.0.co;2, 1979.

675 Holding, J. M., Markager, S., Juul-Pedersen, T., Paulsen, M. L., Møller, E. F., Meire, L. and
676 Sejr, M. K.: Seasonal and spatial patterns of primary production in a high-latitude fjord affected
677 by Greenland Ice Sheet run-off, *Biogeosciences*, 16(19), doi:10.5194/bg-16-3777-2019, 2019.

678 Hopwood, M. J., Carroll, D., Browning, T. J., Meire, L., Mortensen, J., Krisch, S. and
679 Achterberg, E. P.: Non-linear response of summertime marine productivity to increased
680 meltwater discharge around Greenland, *Nat. Commun.*, 9(1), doi:10.1038/s41467-018-05488-8,
681 2018.

682 Hopwood, M. J., Carroll, D., Dunse, T., Hodson, A., Holding, J. M., Iriarte, J. L., Ribeiro, S.,
683 Achterberg, E. P., Cantoni, C., Carlson, D. F., Chierici, M., Clarke, J. S., Cozzi, S., Fransson, A.,
684 Juul-Pedersen, T., Winding, M. S. and Meire, L.: Review Article: How does glacier discharge
685 affect marine biogeochemistry and primary production in the Arctic?, *Cryosph. Discuss.*, (June),
686 1–51, doi:10.5194/tc-2019-136, 2019.

687 Hopwood, M. J., Carroll, D., Dunse, T., Hodson, A., Holding, J. M., Iriarte, J. L., Ribeiro, S.,
688 Achterberg, E. P., Cantoni, C., Carlson, D. F., Chierici, M., Clarke, J. S., Cozzi, S., Fransson, A.,
689 Juul-Pedersen, T., Winding, M. H. S. and Meire, L.: Review article: How does glacier discharge
690 affect marine biogeochemistry and primary production in the Arctic?, *Cryosphere*, 14(4), 1347–
691 1383, doi:10.5194/tc-14-1347-2020, 2020.

692 Høyer, J. L., Karagali, I., Dybkjær, G. and Tonboe, R.: Multi sensor validation and error
693 characteristics of Arctic satellite sea surface temperature observations, *Remote Sens. Environ.*,
694 121, 335–346, doi:10.1016/j.rse.2012.01.013, 2012.

695 Høyer, J. L., Le Borgne, P. and Eastwood, S.: A bias correction method for Arctic satellite sea
696 surface temperature observations, *Remote Sens. Environ.*, 146, 201–213,
697 doi:10.1016/j.rse.2013.04.020, 2014.

698 Hunke, E. C.: Viscous-Plastic Sea Ice Dynamics with the EVP Model: Linearization Issues, *J.*
699 *Comput. Phys.*, 170(1), 18–38, doi:10.1006/jcph.2001.6710, 2001.

700 Hunke, E. C. and Dukowicz, J. K.: An elastic-viscous-plastic model for sea ice dynamics, *J.*
701 *Phys. Oceanogr.*, 27(9), 1849–1867, doi:10.1175/1520-
702 0485(1997)027<1849:AEVPMF>2.0.CO;2, 1997.

703 Ji, R., Jin, M. and Varpe, Ø.: Sea ice phenology and timing of primary production pulses in the
704 Arctic Ocean., *Glob. Chang. Biol.*, 19(3), 734–41, doi:10.1111/gcb.12074, 2013.

705 Juul-Pedersen, T., Arendt, K. E., Mortensen, J., Blicher, M. E., Søgaard, D. H. and Rysgaard,
706 S.: Seasonal and interannual phytoplankton production in a sub-Arctic tidewater outlet glacier
707 fjord, SW Greenland, *Mar. Ecol. Prog. Ser.*, 524(MARCH), 27–38, doi:10.3354/meps11174,
708 2015.

709 Kjeldsen, K. K., Korsgaard, N. J., Bjørk, A. A., Khan, S. A., Box, J. E., Funder, S., Larsen, N.
710 K., Bamber, J. L., Colgan, W., Van Den Broeke, M., Siggaard-Andersen, M. L., Nuth, C.,
711 Schomacker, A., Andresen, C. S., Willerslev, E. and Kjær, K. H.: Spatial and temporal
712 distribution of mass loss from the Greenland Ice Sheet since AD 1900, *Nature*, 528(7582), 396–
713 400, doi:10.1038/nature16183, 2015.

714 Large, W. G. and Yeager, S. G.: The global climatology of an interannually varying air - Sea
715 flux data set, *Clim. Dyn.*, 33(2–3), 341–364, doi:10.1007/s00382-008-0441-3, 2009.

716 Larsen, J. (2022). FlexSem source code (2022-01-31). Zenodo.
717 <https://doi.org/10.5281/zenodo.7124459>

718 Lavergne, T., Macdonald Sørensen, A., Kern, S., Tonboe, R., Notz, D., Aaboe, S., Bell, L.,
719 Dybkjær, G., Eastwood, S., Gabarro, C., Heygster, G., Anne Killie, M., Brandt Kreiner, M.,

720 Lavelle, J., Saldo, R., Sandven, S. and Pedersen, L. T.: Version 2 of the EUMETSAT OSI SAF
721 and ESA CCI sea-ice concentration climate data records, *Cryosphere*, 13(1), doi:10.5194/tc-13-
722 49-2019, 2019.

723 Leu, E., Mundy, C. J. J., Assmy, P., Campbell, K., Gabrielsen, T. M. M., Gosselin, M., Juul-
724 Pedersen, T. and Gradinger, R.: Arctic spring awakening - Steering principles behind the
725 phenology of vernal ice algal blooms, *Prog. Oceanogr.*, 139, 151–170,
726 doi:10.1016/j.pocean.2015.07.012, 2015.

727 Levinsen, H. and Nielsen, T. G.: The trophic role of marine pelagic ciliates and heterotrophic
728 dinoflagellates in arctic and temperate coastal ecosystems: A cross-latitude comparison, *Limnol.*
729 *Oceanogr.*, 47(2), 427–439, doi:10.4319/lo.2002.47.2.0427, 2002.

730 Levinsen, H., Nielsen, T. G. and Hansen, B. W.: Annual succession of marine pelagic protozoans
731 in Disko Bay, West Greenland, with emphasis on winter dynamics, *Mar. Ecol. Prog. Ser.*, 206,
732 119–134, doi:10.3354/meps206119, 2000.

733 Lovejoy, C., Vincent, W. F., Bonilla, S., Roy, S., Martineau, M. J., Terrado, R., Potvin, M.,
734 Massana, R. and Pedrós-Alió, C.: Distribution, phylogeny, and growth of cold-adapted
735 picoprasinophytes in arctic seas, *J. Phycol.*, 43(1), 78–89, doi:10.1111/j.1529-
736 8817.2006.00310.x, 2007.

737 Lydersen, C., Assmy, P., Falk-Petersen, S., Kohler, J., Kovacs, K. M., Reigstad, M., Steen, H.,
738 Strøm, H., Sundfjord, A., Varpe, Ø., Walczowski, W., Weslawski, J. M. and Zajaczkowski, M.:
739 The importance of tidewater glaciers for marine mammals and seabirds in Svalbard, Norway, *J.*
740 *Mar. Syst.*, 129, 452–471, doi:10.1016/j.jmarsys.2013.09.006, 2014.

741 Maar, M., Møller, E. F., Larsen, J., Madsen, K. S., Wan, Z., She, J., Jonasson, L. and Neumann,
742 T.: Ecosystem modelling across a salinity gradient from the North Sea to the Baltic Sea, *Ecol.*
743 *Modell.*, 222(10), 1696–1711, doi:10.1016/j.ecolmodel.2011.03.006, 2011.

744 Maar, M., Markager, S., Madsen, K. S., Windolf, J., Lyngsgaard, M. M., Andersen, H. E. and
745 Møller, E. F.: The importance of local versus external nutrient loads for Chl a and primary
746 production in the Western Baltic Sea, *Ecol. Modell.*, 320, doi:10.1016/j.ecolmodel.2015.09.023,
747 2016.

748 Maar, M. Møller, E.F., Larsen J. (2022). FlexSem Biogeochemical model for Disko Bay,
749 Greenland. (Version v16). Zenodo. <https://doi.org/10.5281/zenodo.7401870>

750 Madsen, K. S., Rasmussen, T. A. S., Ribergaard, M. H. and Ringgaard, I. M.: High resolution
751 sea-ice modelling and validation of the Arctic with focus on South Greenland Waters, 2004-
752 2013, *Polarforschung*, 85(2), 101–105, doi:10.2312/polfor.2016.006, 2016.

753 Mankoff, K. D., Straneo, F., Cenedese, C., Das, S. B., Richards, C. G. and Singh, H.: Structure
754 and dynamics of a subglacial discharge plume in a Greenlandic fjord, *J. Geophys.*
755 *Res. Ocean.*, 121(12), 8670–8688, doi:10.1002/2016JC011764, 2016.

756 Mankoff, K. D., Solgaard, A., Colgan, W., Ahlstrøm, A. P., Abbas Khan, S. and Fausto, R. S.:
757 Greenland Ice Sheet solid ice discharge from 1986 through March 2020, *Earth Syst. Sci. Data*,
758 12(2), 1367–1383, doi:10.5194/essd-12-1367-2020, 2020a.

759 Mankoff, K. D., Ahlstrøm, A. P., Colgan, W., Faust, R. S., Fettweis, X., Kondo, K., Langley, K.,
760 Noël, B., Sugiyama, S. and As, D. van: Greenland liquid water runoff from 1979 through 2017,
761 *Earth Syst. Sci. Data*, (April), doi:doi.org/10.5194/essd-2020-47, 2020b.

762 Mankoff, K. D., Fettweis, X., Langen, P. L., Stendel, M., Kjeldsen, K. K., Karlsson, N. B., Noël,
763 B., van den Broeke, M. R., Solgaard, A., Colgan, W., Box, J. E., Simonsen, S. B., King, M. D.,
764 Ahlstrøm, A. P., Andersen, S. B. and Fausto, R. S.: Greenland ice sheet mass balance from 1840
765 through next week, *Earth Syst. Sci. Data*, 13(10), 5001–5025, doi:10.5194/essd-13-5001-2021,
766 2021.

767 Massicotte, P., Peeken, I., Katlein, C., Flores, H., Huot, Y., Castellani, G., Arndt, S., Lange, B.
768 A., Tremblay, J.-É. and Babin, M.: Sensitivity of phytoplankton primary production estimates to
769 available irradiance under heterogeneous sea-ice conditions, *J. Geophys. Res. Ocean.*, (June),
770 doi:10.1029/2019JC015007, 2019.

771 Meier, W. N., Hovelsrud, G. K., van Oort, B. E. H., Key, J. R., Kovacs, K. M., Michel, C., Haas,
772 C., Granskog, M. A., Gerland, S., Perovich, D. K., Makshtas, A. and Reist, J. D.: Arctic sea ice
773 in transformation: A review of recent observed changes and impacts on biology and human
774 activity, *Rev. Geophys.*, 52(3), 185–217, doi:10.1002/2013RG000431, 2014.

775 Meire, L., Mortensen, J., Meire, P., Juul-Pedersen, T., Sejr, M. K., Rysgaard, S., Nygaard, R.,

776 Huybrechts, P. and Meysman, F. J. R.: Marine-terminating glaciers sustain high productivity in
777 Greenland fjords, *Glob. Chang. Biol.*, 23(12), 5344–5357, doi:10.1111/gcb.13801, 2017.

778 Menden-Deuer, S., Lawrence, C. and Franzè, G.: Herbivorous protist growth and grazing rates at
779 in situ and artificially elevated temperatures during an Arctic phytoplankton spring bloom, *PeerJ*,
780 2018(7), doi:10.7717/peerj.5264, 2018.

781 Møller, E. F. and Nielsen, T. G.: Borealization of Arctic zooplankton — smaller and less fat
782 zooplankton species in Disko Bay, Western Greenland, , 1–14, doi:10.1002/Ino.11380, 2019.

783 Møller, E. F. and Nielsen, T. G.: Borealization of Arctic zooplankton—smaller and less fat
784 zooplankton species in Disko Bay, Western Greenland, *Limnol. Oceanogr.*, 65(6), 1175–1188,
785 doi:10.1002/Ino.11380, 2020.

786 Møller, E. F. E. F., Maar, M., Jónasdóttir, S. H. S. H., Gissel Nielsen, T. and Tönnesson, K.: The
787 effect of changes in temperature and food on the development of *Calanus finmarchicus* and
788 *Calanus helgolandicus* populations, *Limnol. Oceanogr.*, 57(1), 211–220,
789 doi:10.4319/lo.2012.57.1.0211, 2012.

790 Møller, E. F. E. F., Bohr, M., Kjellerup, S., Maar, M., Møhl, M., Swalethorp, R. and Nielsen, T.
791 G. T. G.: *Calanus finmarchicus* egg production at its northern border, *J. Plankton Res.*, 38(5),
792 1206–1214, doi:10.1093/plankt/fbw048, 2016.

793 Møller, E.F., Nielsen, T.G. (2022). Borealization of Arctic zooplankton—smaller and less fat
794 zooplankton species in Disko Bay, Western Greenland [Data set]. Zenodo.
795 <https://doi.org/10.5281/zenodo.745457>

796 Møller, E.F., Christensen, A., Larsen, J., Mankoff, K. D., Ribergaard, M. H., Sejr, M. K.,
797 Wallhead, P., Maar, M (2022). The sensitivity of primary productivity in Disko Bay, a coastal
798 Arctic ecosystem to changes in freshwater discharge and sea ice cover [Data set]. Zenodo.
799 <https://doi.org/10.5281/zenodo.7454727>

800 Morlighem, M., Williams, C. N., Rignot, E., An, L., Arndt, J. E., Bamber, J. L., Catania, G.,
801 Chauché, N., Dowdeswell, J. A., Dorschel, B., Fenty, I., Hogan, K., Howat, I., Hubbard, A.,
802 Jakobsson, M., Jordan, T. M., Kjeldsen, K. K., Millan, R., Mayer, L., Mouginot, J., Noël, B. P.
803 Y., O’Cofaigh, C., Palmer, S., Rysgaard, S., Seroussi, H., Siegert, M. J., Slabon, P., Straneo, F.,

804 van den Broeke, M. R., Weinrebe, W., Wood, M. and Zinglensen, K. B.: BedMachine v3:
805 Complete Bed Topography and Ocean Bathymetry Mapping of Greenland From Multibeam
806 Echo Sounding Combined With Mass Conservation, *Geophys. Res. Lett.*, 44(21), 11,051-11,061,
807 doi:10.1002/2017GL074954, 2017.

808 Mortensen, J., Rysgaard, S., Bendtsen, J., Lennert, K., Kanzow, T., Lund, H. and Meire, L.:
809 Subglacial Discharge and Its Down-Fjord Transformation in West Greenland Fjords With an Ice
810 Mélange, *J. Geophys. Res. Ocean.*, 125(9), 1–13, doi:10.1029/2020JC016301, 2020.

811 Mouginot, J., Rignot, E., Bjørk, A. A., van den Broeke, M., Millan, R., Morlighem, M., Noël, B.,
812 Scheuchl, B. and Wood, M.: Forty-six years of Greenland Ice Sheet mass balance from 1972 to
813 2018, *Proc. Natl. Acad. Sci. U. S. A.*, 116(19), 9239–9244, doi:10.1073/pnas.1904242116, 2019.

814 Murray, C., Markager, S., Stedmon, C. A., Juul-Pedersen, T., Sejr, M. K. and Bruhn, A.: The
815 influence of glacial melt water on bio-optical properties in two contrasting Greenlandic fjords,
816 *Estuar. Coast. Shelf Sci.*, 163(PB), 72–83, doi:10.1016/j.ecss.2015.05.041, 2015.

817 Neumann, T.: Towards a 3D-ecosystem model of the Baltic Sea, *J. Mar. Syst.*, 25(3–4), 405–
818 419, doi:10.1016/S0924-7963(00)00030-0, 2000.

819 Pabi, S., van Dijken, G. L. and Arrigo, K. R.: Primary production in the Arctic Ocean, 1998-
820 2006, *J. Geophys. Res. Ocean.*, 113(8), 1998–2006, doi:10.1029/2007JC004578, 2008.

821 Randelhoff, A., Holding, J., Janout, M., Sejr, M. K., Babin, M., Tremblay, J.-éric, Alkire, M. B.
822 and Oliver, H.: Pan-Arctic Ocean Primary Production Constrained by Turbulent Nitrate Fluxes, ,
823 7(March), 1–15, doi:10.3389/fmars.2020.00150, 2020.

824 Rasmussen, T. A. S., Høyer, J. L., Ghent, D., Bulgin, C. E., Dybkjær, G., Ribergaard, M. H.,
825 Nielsen-Englyst, P. and Madsen, K. S.: Impact of Assimilation of Sea-Ice Surface Temperatures
826 on a Coupled Ocean and Sea-Ice Model, *J. Geophys. Res. Ocean.*, 123(4), 2440–2460,
827 doi:10.1002/2017JC013481, 2018.

828 Ross, O. N. and Geider, R. J.: New cell-based model of photosynthesis and photo-acclimation:
829 accumulation and mobilisation of energy reserves in phytoplankton, *Mar. Ecol. Prog. Ser.*, 383,
830 53–71, doi:10.3354/meps07961, 2009.

831 Rysgaard, S., Boone, W., Carlson, D., Sejr, M. K., Bendtsen, J., Juul-Pedersen, T., Lund, H.,

832 Meire, L. and Mortensen, J.: An Updated View on Water Masses on the pan-West Greenland
833 Continental Shelf and Their Link to Proglacial Fjords, *J. Geophys. Res. Ocean.*, 125(2), 0–3,
834 doi:10.1029/2019JC015564, 2020.

835 Sejr, M. K., Nielsen, T. G., Rysgaard, S., Risgaard-petersen, N., Sturluson, M. and Blicher, M.
836 E.: Fate of pelagic organic carbon and importance of pelagic – benthic coupling in a shallow
837 cove, *Mar. Ecol. Prog. Ser.*, 341, 75–88, 2007.

838 Shchepetkin, A. F. and McWilliams, J. C.: The regional oceanic modeling system (ROMS): A
839 split-explicit, free-surface, topography-following-coordinate oceanic model, *Ocean Model.*, 9(4),
840 347–404, doi:10.1016/j.ocemod.2004.08.002, 2005.

841 Steele, M., Morley, R. and Ermold, W.: PHC: A global ocean hydrography with a high-quality
842 Arctic Ocean, *J. Clim.*, 14(9), 2079–2087, doi:10.1175/1520-
843 0442(2001)014<2079:PAGOHW>2.0.CO;2, 2001.

844 Stroeve, J. C., Markus, T., Boisvert, L., Miller, J. and Barrett, A.: Changes in Arctic melt season
845 and implications for sea ice loss, *Geophys. Res. Lett.*, 41(4), 1216–1225,
846 doi:10.1002/2013GL058951, 2014.

847 Swailethorp, R., Kjellerup, S., Dünweber, M., Nielsen, T., Møller, E., Rysgaard, S. and Hansen,
848 B.: Grazing, egg production, and biochemical evidence of differences in the life strategies of
849 *Calanus finmarchicus*, *C. glacialis* and *C. hyperboreus* in Disko Bay, western Greenland, *Mar.*
850 *Ecol. Prog. Ser.*, 429, 125–144, doi:10.3354/meps09065, 2011.

851 Thomas, D. N., Baumann, M. E. M. and Gleitz, M.: Efficiency of carbon assimilation and
852 photoacclimation in a small unicellular *Chaetoceros* species from the Weddell Sea (Antarctica):
853 influence of temperature and irradiance, *J. Exp. Mar. Bio. Ecol.*, 157(2), 195–209,
854 doi:10.1016/0022-0981(92)90162-4, 1992.

855 Thyrring, J., Wegeberg, S., Blicher, M. E., Krause-Jensen, D., Høgslund, S., Olesen, B., Jozef,
856 W., Mouritsen, K. N., Peck, L. S. and Sejr, M. K.: Latitudinal patterns in intertidal ecosystem
857 structure in West Greenland suggest resilience to climate change, *Ecography (Cop.)*, 44(8),
858 1156–1168, doi:10.1111/ecog.05381, 2021.

859 Tremblay, J.-É. and Gagnon, J.: The effects of irradiance and nutrient supply on the productivity

860 of Arctic waters: a perspective on climate change, in *Influence of Climate Change on the*
861 *Changing Arctic and Sub-Arctic Conditions*, pp. 73–93, Springer Netherlands, Dordrecht., 2009.

862 Tremblay, J. É., Anderson, L. G., Matrai, P., Coupel, P., Bélanger, S., Michel, C. and Reigstad,
863 M.: Global and regional drivers of nutrient supply, primary production and CO₂ drawdown in
864 the changing Arctic Ocean, *Prog. Oceanogr.*, 139, 171–196, doi:10.1016/j.pocean.2015.08.009,
865 2015.

866 Vernet, M., Ellingsen, I., Marchese, C., Bélanger, S., Cape, M., Slagstad, D. and Matrai, P. A.:
867 Spatial variability in rates of Net Primary Production (NPP) and onset of the spring bloom in
868 Greenland shelf waters, *Prog. Oceanogr.*, 198(September 2020), 102655,
869 doi:10.1016/j.pocean.2021.102655, 2021.

870 Yang, X., Petersen, C., Amstrup B., Andersen, B. S., Hansen, Feddersen, H., Kmit, M.,
871 Korsholm, U., Lindberg, K., Mogensen, K., Sass, B.H., Sattler, K., Nielsen, N.W.: The DMI-
872 HIRLAM upgrade in June 2004. DMI-Tech. Rep. 05-09, Danish Meteorological Institute,
873 Copenhagen, Denmark, 2005.

874 Yang, X., Palmason, B., Andersen, B. S., Hansen Sass, B., Amstrup, B., Dahlbom, M., Petersen,
875 C., Pagh Nielsen, K., Mottram, R., Woetmann, N., Mahura, A. Thorsteinsson, S., Nawri, N., and
876 Petersen, G. N. 2017: IGA, the Joint Operational HARMONIE by DMI and IMO, ALADIN-
877 HIRLAM Newsletter, No. 8, 87–94, 2017.

878 Yang, X., Palmason, B., Sattler, K., Thorsteinsson, S., Amstrup, B., Dahlbom, M, Hansen Sass,
879 B., Pagh Nielsen, K., Petersen, G. N. 2018: IGB, the Upgrade to the Joint Operational
880 HARMONIE by DMI and IMO in 2018, ALADIN-HIRLAM Newsletter, No. 11, 93-96, 2018.

881 Zhang, J., Spitz, Y. H., Steele, M., Ashjian, C., Campbell, R., Berline, L. and Matrai, P.:
882 Modeling the impact of declining sea ice on the Arctic marine planktonic ecosystem, *J. Geophys.*
883 *Res. Ocean.*, 115(10), doi:10.1029/2009JC005387, 2010.

884

885

886 **8 Tables**

887 Table 1: Characteristics of the reference model runs of 2010 and 2017, and the annual average
 888 NPP in the bay obtained from scenarios runs with changes in the sea ice cover and the freshwater
 889 discharge (Figure 8 and 9). SD are the standard variation between the different model grid cells.

				2010	2017
Reference	Average annual primary production	gC m ⁻² yr ⁻¹		147 ±41	90 ±28
	Average annual discharge	m ³ s ⁻¹		6275	4058
	Average annual sea ice cover, March-April	%		24	79
Scenarios	Average annual primary production	gC m ⁻² yr ⁻¹	No sea ice	150 ±50	120 ±35
			No freshwater discharge	144 ±53	90 ±46
			No sea ice, No freshwater discharge	147 ±47	119 ±32
			2 x freshwater discharge	149 ±48	90 ±45
			No sea ice, 2 x freshwater discharge	152 ±53	122 ±35

890

891 Table 2: Statistics for seasonal comparison between observational data (monthly climatology)
 892 and model data (monthly average from 2005 to 2018) at the Disko Bay Station. $N=12$ for
 893 copepods, $N=11$ for temperature, salinity and *Chl a* and $N=10$ for other variables (see Figure 4).
 894 All correlations were significant ($p<0.01$).

895

	Unit	Model error	RMSE	Correlation	<i>cf</i>
Temperature	°C	-0.28	0.96	0.94	0.31
Salinity	-	-0.09	0.21	0.79	0.56
NO ₃	mmol m ⁻³	0.00	1.43	0.87	0.39
Silicate	mmol m ⁻³	0.78	1.70	0.83	0.66
Phosphate	mmol m ⁻³	-0.01	0.12	0.82	0.46
<i>Chl a</i>	mg m ⁻³	0.03	0.97	0.87	0.37
Copepod biomass	mgC m ⁻³	0.83	4.66	0.94	0.23

896

897 Table 3: Statistics for the spatial comparison between remote sensing data and surface model
 898 data for spring (April-June) and summer (July-September) in 2010 and 2017. In spring 2017,
 899 only June is included due to ice cover in April-May. $N=6145$, and all correlations were
 900 significant ($p<0.01$).

	Model error	RMSE	Correlatio n	cf
<i>Surface temperature</i>				
2010 spring	0.8	1.3	0.45	1.0
2010 summer	-1.4	2.0	0.14	1.5
2017 spring	0.8	1.4	0.58	0.9
2017 summer	-2.0	2.3	0.33	0.2
<i>Log₁₀ (Chl a [mg/m³])</i>				
2010 spring	0.6	0.7	0.30	0.4
2010 summer	0.5	0.8	0.33	0.2
2017 spring	1.7	1.8	0.29	1.7
2017 summer	0.9	1.1	0.46	1.2

901

902 9 Figures

903 Figure 1: Map of Disko Bay with the bathymetry, the Flexsem model grid, position of
904 freshwater sources (red dots: land runoff, red dots with black circle: land + ice runoff), position
905 of two stations presented in more detail, and the area used for calculation of the average Disko
906 Bay primary production (red box).

907 Figure 2: Development in freshwater discharge and sea ice cover over time. a) Freshwater
908 discharge from the Greenland ice sheet divided into liquid from precipitation over land (Land
909 runoff), liquid deriving from melt from the Greenland Ice sheet/glaciers (Ice runoff) and ice
910 deriving directly from the glacier (solid ice) 1960 to 2019, and b) number of days with more than
911 40% sea ice cover from 1986 to 2019, derived from satellite measurement (AICE), by the sea ice
912 model providing input to the this study (CICE), and by visual observation at Arctic Station,
913 Qeqertarsuaq (AS).

914 Figure 3: Primary production, sea ice cover and freshwater discharge in Disko Bay from 2004 to
915 2018. Primary production and sea ice cover are assessed in the red square in Fig 1, whereas the
916 freshwater discharge are from the full model domain. (a) Average annual primary production (gC
917 $\text{m}^{-2} \text{ year}^{-1}$) \pm SD (variation between model grid cells), (b) the average monthly primary
918 production ($\text{mgC m}^{-2} \text{ day}^{-1}$) \pm SD (variation between years), light is average from Arctic station
919 (2010-2019), (c) the annual average sea ice cover in March and April (%), (d) the average
920 monthly sea ice cover (%), (e) the average annual freshwater discharge ($\text{m}^3 \text{ s}^{-1}$), and (f) the
921 average monthly freshwater discharge ($1000 \text{ m}^3 \text{ s}^{-1}$).

922 Figure 4: Comparison of monthly means (\pm SD) of observations and model data (2004-2018) at
923 $69^{\circ}14'N$, $53^{\circ}23'W$ for (a) temperature ($^{\circ}C$), (b) salinity, (c) nitrate (mmol m^{-3}), (d) silicate
924 (mmol m^{-3}), (e) phosphate (mmol m^{-3}), (f) Chl *a*, (mg m^{-3}), (g) microzooplankton biomass (mgC
925 m^{-3}), and (h) mesozooplankton biomass (mgC m^{-3}). Means are averaged over 0-20 m depth,
926 except for mesozooplankton which it is 0-50 m.

927 Figure 5: Sea ice cover (%), average nitrate concentration in 0-30 m (mmol m^{-3}) average Chl *a*
928 concentration in 0-30 m (mg m^{-3}) and primary production ($\text{mgC m}^{-2} \text{ d}^{-1}$) at a station in open Bay
929 (Bay Station) and at one close to the glacier (Glacier Station) (Fig. 1) in 2010 and 2017.

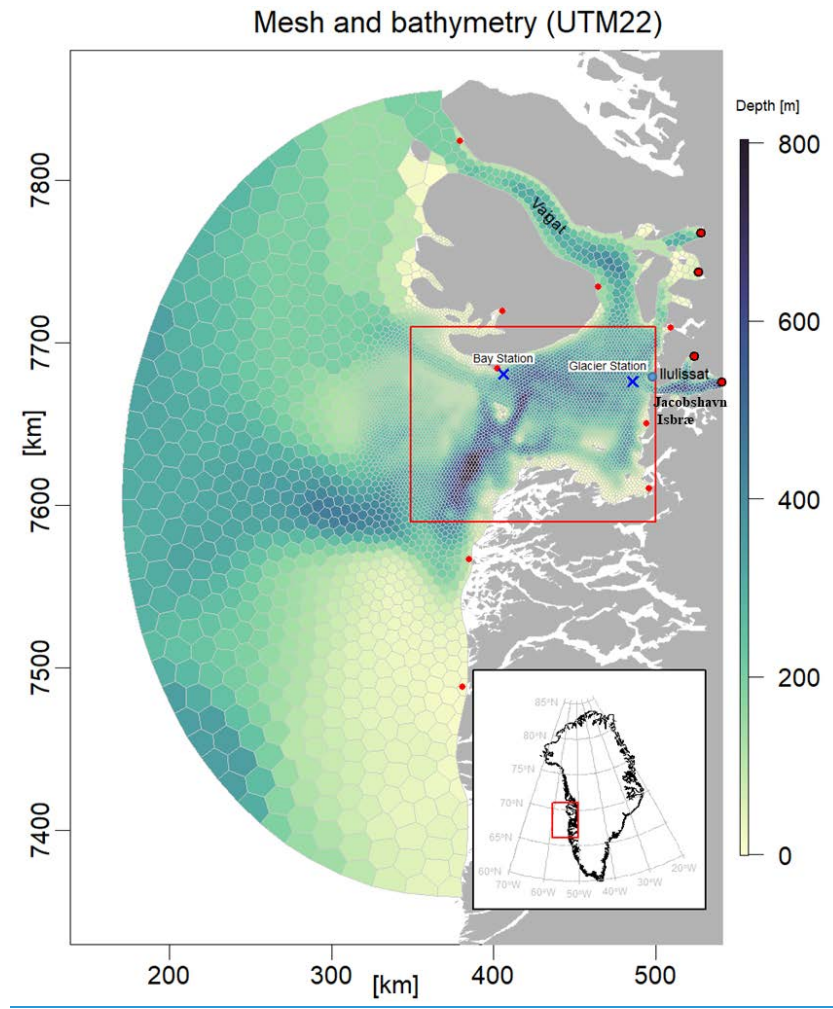
930 Figure 6: Average spatial distribution of primary production (gC m^{-2}) in 2010 and 2017
931 respectively for the periods A)+D) March-October, B)+E) March-June and C) +F) July-October.

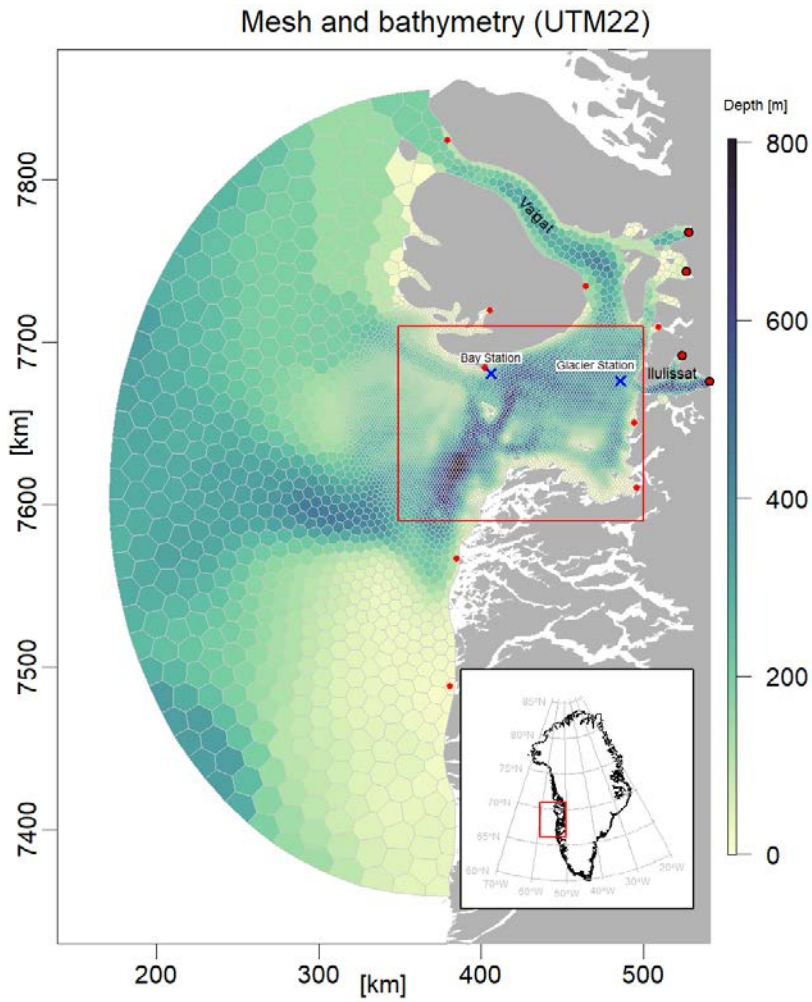
932 Figure 7: Correlation coefficients between the annual primary production (a) and average sea ice
933 cover in March-April and (b) and surface salinity across the period 2004-2018.

934 Figure 8: Response of the annual primary production to simple scenarios of changes in sea ice
935 cover and freshwater discharge (Q) in 2010 expressed as percentage change relative to the
936 standard model run. The percentages in the bottom of the figure are the changes in primary
937 production in the total area shown. The following model scenarios were run (Table 1): (a)
938 standard model run, (b) assuming no sea ice cover, (c) assuming no freshwater discharge from
939 the Greenland ice sheet, (d) the combination of (b) and (c), (e) assuming 2 times the freshwater
940 discharge of the standard run, and (f) the combination of (b) and (e).

941 Figure 9: Response of the annual primary production to simple scenarios of changes in sea ice
942 cover and freshwater discharge (Q) in 2017 expressed as percentage change relative to the
943 standard model run. The percentages in the bottom of the figure are the changes in primary
944 production in the total area shown. The following model scenarios were run (Table 1): (a)
945 standard model run, (b) assuming no sea ice cover, (c) assuming no freshwater discharge from
946 the Greenland ice sheet, (d) the combination of (b) and (c), (e) assuming 2 times the freshwater
947 discharge of the standard run, and (f) the combination of (b) and (e).

Figure 1: Map of Disko Bay with the bathymetry, the Flexsem model grid, position of freshwater sources (red dots: land runoff, red dots with black circle: land + ice runoff), position of two stations presented in more detail, and the area used for calculation of the average Disko Bay primary production (red box).





948
949

Figure 2: Development in freshwater discharge and sea ice cover over time. a) Freshwater discharge from the Greenland ice sheet divided into liquid from precipitation over land (Land runoff), liquid deriving from melt from the Greenland Ice sheet/glaciers (Ice runoff) and ice deriving directly from the glacier (solid ice) 1960 to 2019, and b) number of days with more than 40% sea ice cover from 1986 to 2019, derived from satellite measurement (AICE), by the

sea ice model providing input to the this study (CICE), and by visual observation at Arctic Station, Qeqertarsuaq (AS).

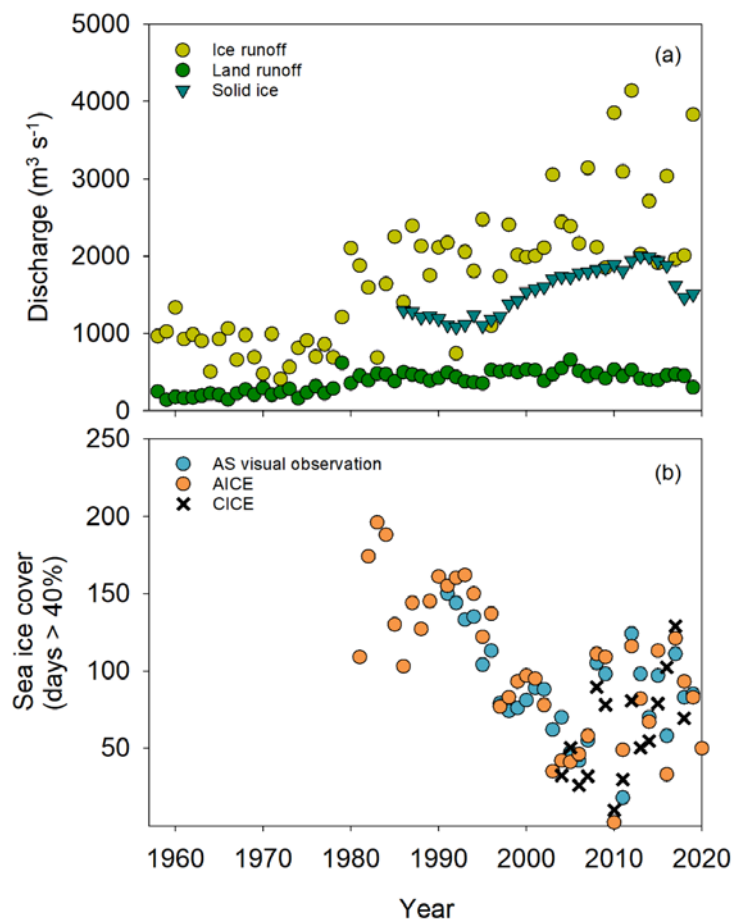


Figure 3: Primary production, sea ice cover and freshwater discharge in Disko Bay from 2004 to 2018. Primary production and sea ice cover are assessed in the red square in Fig 1, whereas the freshwater discharge are from the full model domain. (a) Average annual primary production ($\text{gC m}^{-2} \text{ year}^{-1}$) \pm SD (variation between model grid cells), (b) the average monthly primary production ($\text{mgC m}^{-2} \text{ day}^{-1}$) \pm SD (variation between years), light is average from Arctic station (2010-2019), (c) the annual average sea ice cover in March and April (%), (d) the average monthly sea ice cover (%), (e) the average annual freshwater discharge ($\text{m}^3 \text{ s}^{-1}$), and (f) the average monthly freshwater discharge ($1000 \text{ m}^3 \text{ s}^{-1}$).

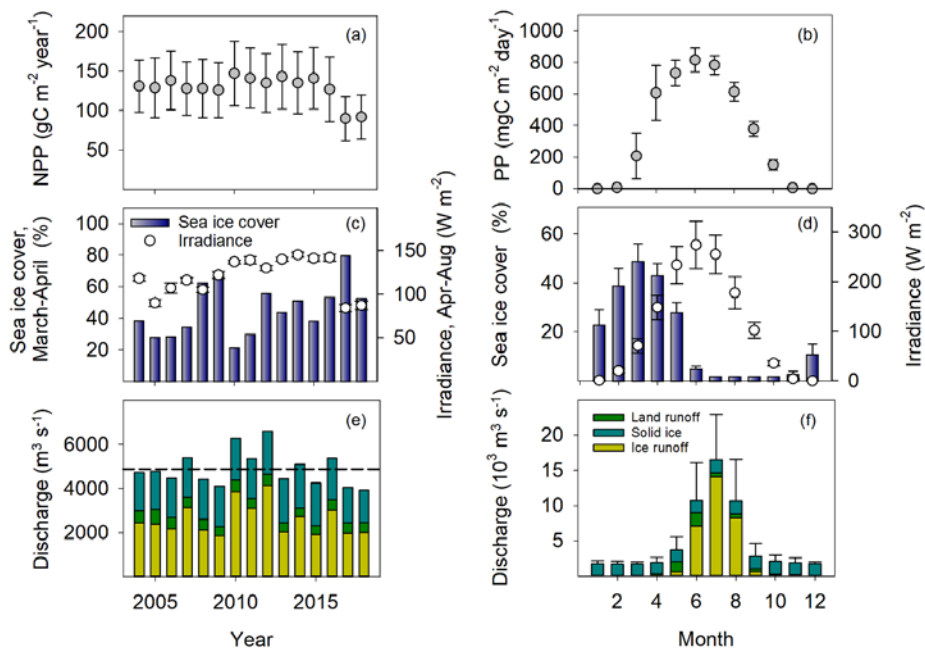
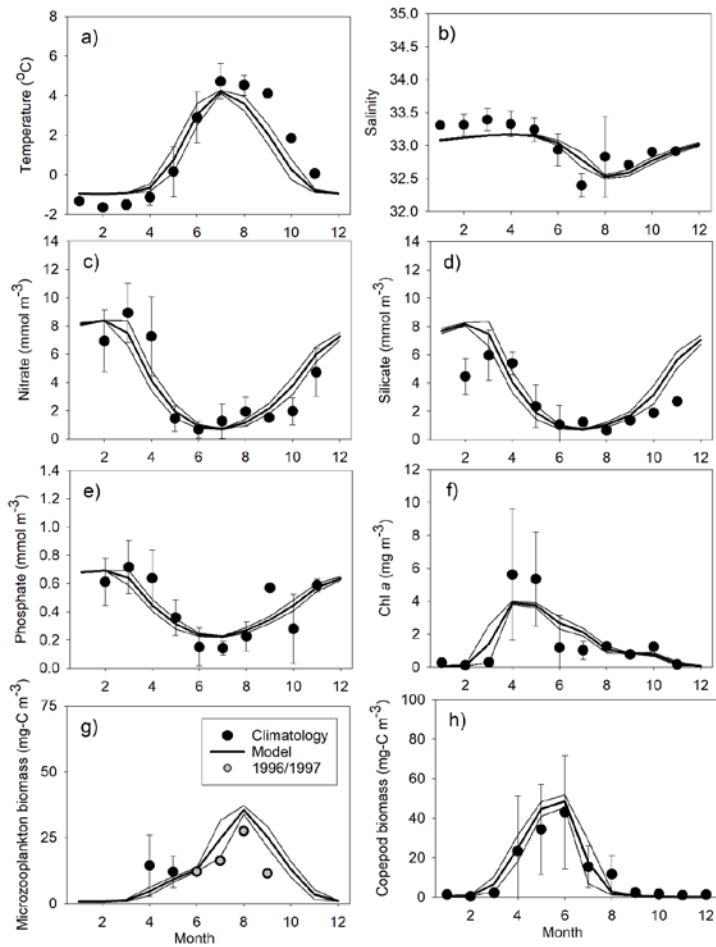


Figure 4: Comparison of monthly means (\pm SD) of observations and model data (2004-2018) at 69°14'N, 53°23'W for (a) temperature ($^{\circ}$ C), (b) salinity, (c) nitrate (mmol m^{-3}), (d) silicate (mmol m^{-3}), (e) phosphate (mmol m^{-3}), (f) Chl *a*, (mg m^{-3}), (g) microzooplankton biomass (mgC m^{-3}), and (h) mesozooplankton biomass (mgC m^{-3}). Means are averaged over 0-20 m depth, except for mesozooplankton which it is 0-50 m. Means are averaged over 0-20 m depth, except for mesozooplankton which it is 0-50 m.



952

953

Fig 5: Sea ice cover (%), average nitrate concentration in 0-30 m (mmol m^{-3}) average Chl *a* concentration in 0-30 m (mg m^{-3}) and primary production ($\text{mgC m}^{-2} \text{d}^{-1}$) at a station in open Bay (Bay Station) and at one close to the glacier (Glacier Station) (Fig. 1) in 2010 and 2017.

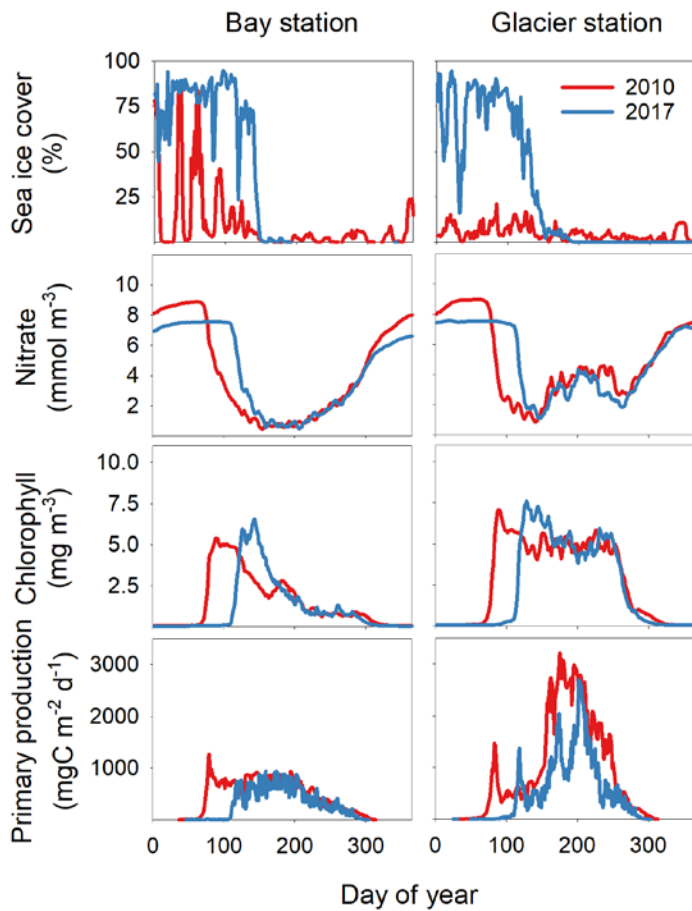


Fig 6: Average spatial distribution of primary production (gC m^{-2}) in 2010 and 2017 respectively for the periods A)+D) March-October, B)+E) March-June and C) +F) July-October.

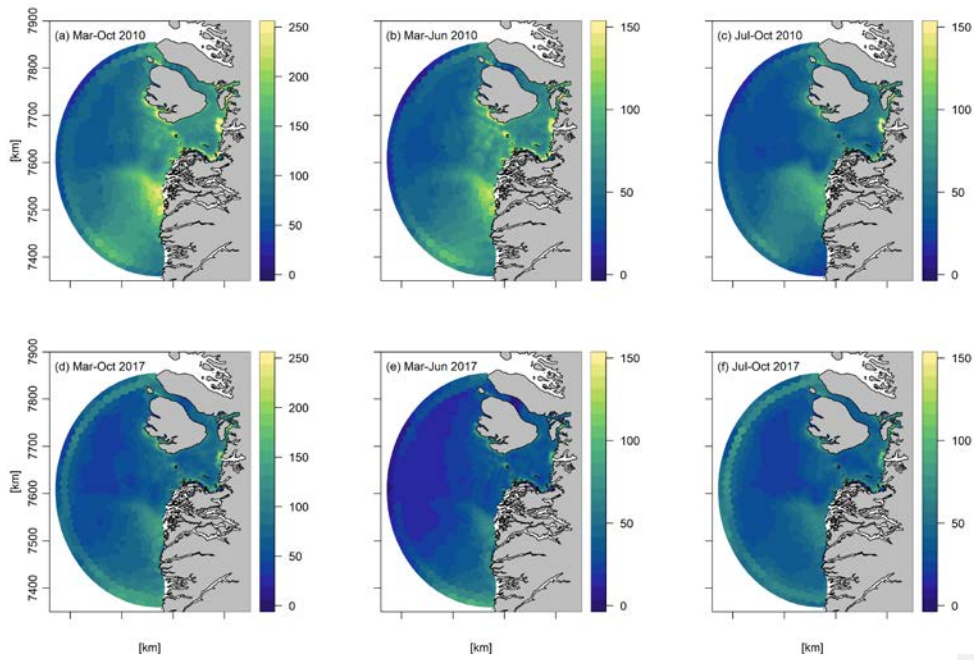


Fig 7: Correlation coefficients between the annual primary production (a) and average sea ice cover in March-April and (b) and surface salinity across the period 2004-2018.

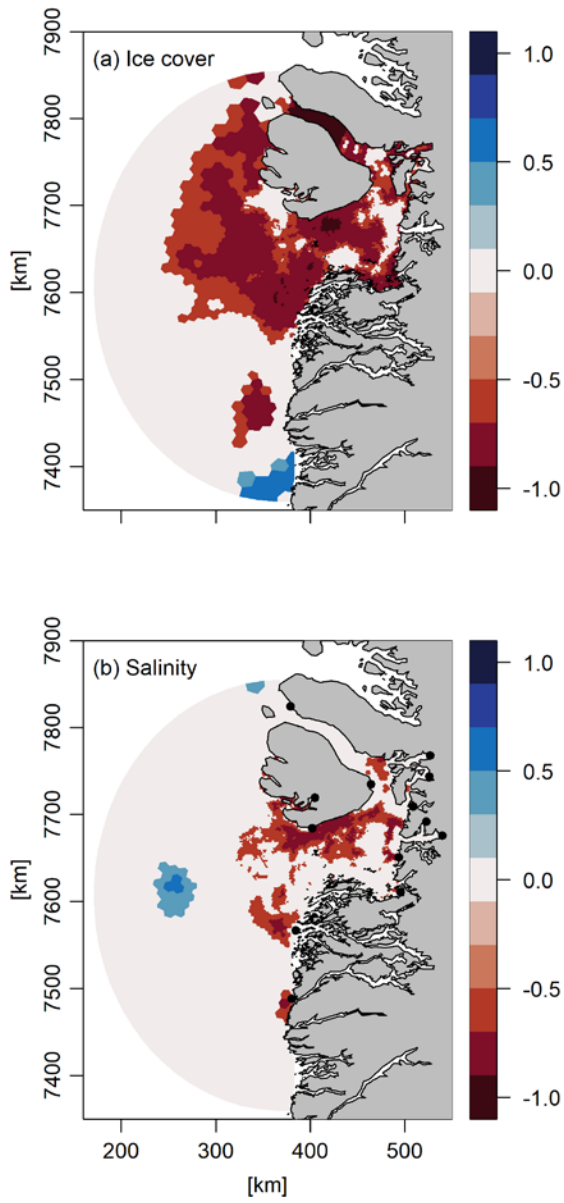


Fig 8: Response of the annual primary production to simple scenarios of changes in sea ice cover and freshwater discharge (Q) in 2010 expressed as percentage change relative to the standard model run. The percentages in the bottom of the figure are the changes in primary production in the total area shown. The following model scenarios were run (Table 1): (a) standard model run, (b) assuming no sea ice cover, (c) assuming no freshwater discharge from the Greenland ice sheet, (d) the combination of (b) and (c), (e) assuming 2 times the freshwater discharge of the standard run, and (f) the combination of (b) and (e).

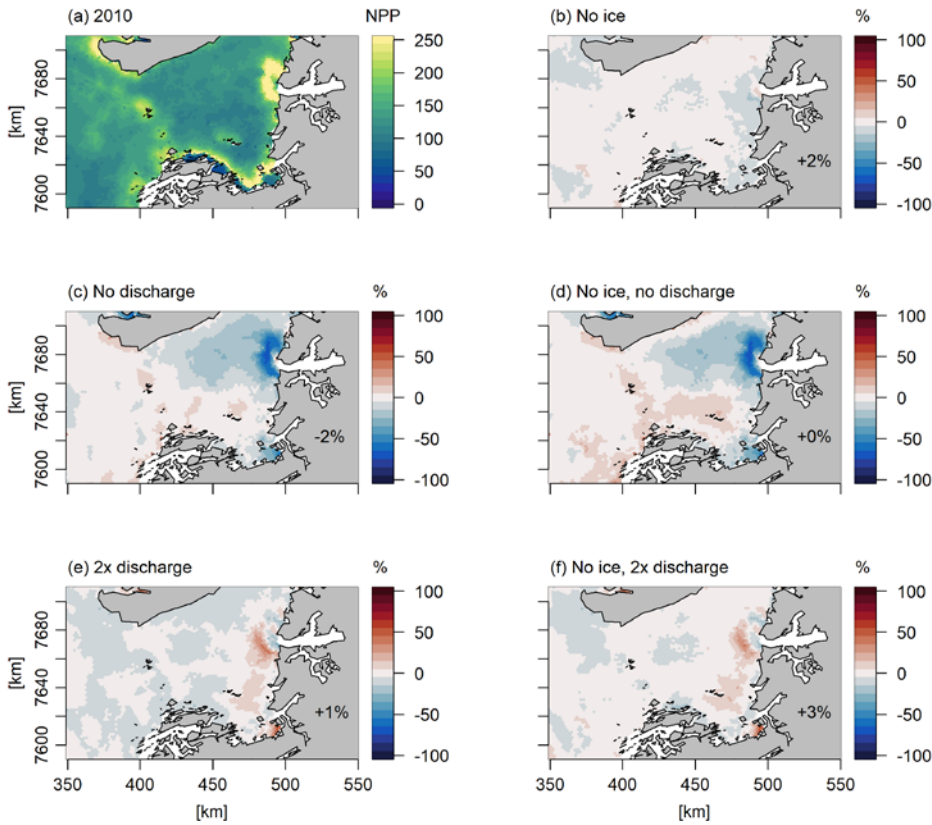
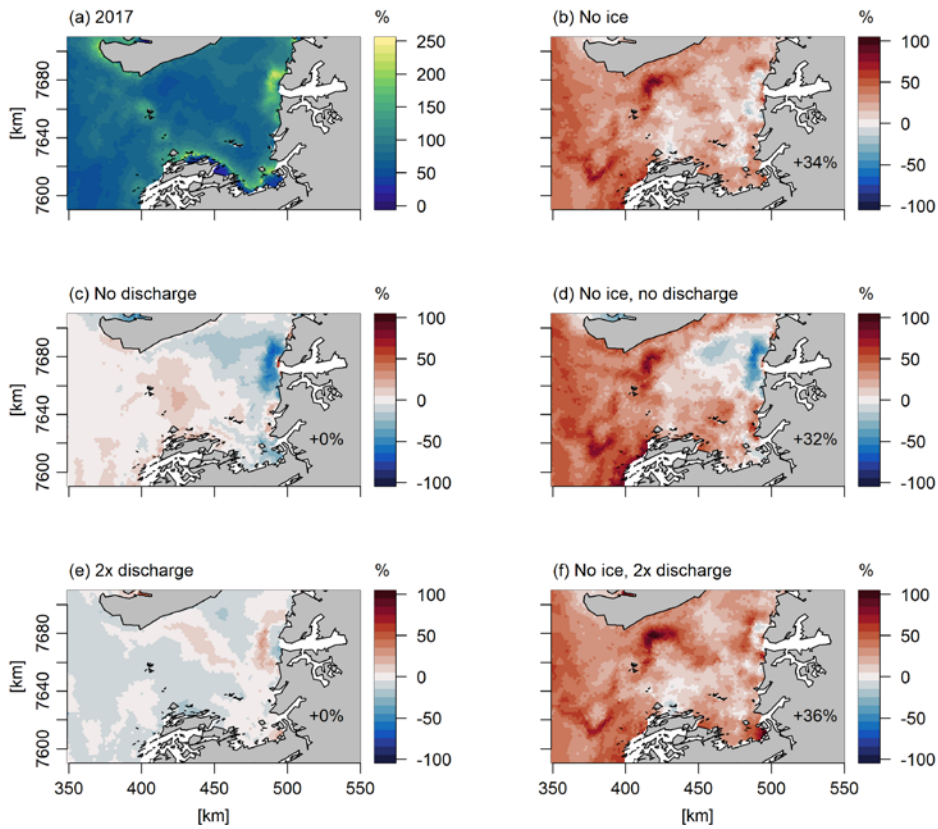


Fig 9: Response of the annual primary production to simple scenarios of changes in sea ice cover and freshwater discharge (Q) in 2017 expressed as percentage change relative to the standard model run. The percentages in the bottom of the figure are the changes in primary production in the total area shown. The following model scenarios were run (Table 1): (a) standard model run, (b) assuming no sea ice cover, (c) assuming no freshwater discharge from the Greenland ice sheet, (d) the combination of (b) and (c), (e) assuming 2 times the freshwater discharge of the standard run, and (f) the combination of (b) and (e).



958 10 Appendices

959 10.1 Appendix A, Ecological model constants

960 Table A.1. Constants in the FlexSem ecological Disko Bay model.

Parameter	Description	Numerical value	Units
Phytoplankton			
α_1	Half-saturation uptake diatoms	0.55	mmol-N m ⁻³
α_2	Half-saturation uptake flagellates	0.45	mmol-N m ⁻³
RD_0	Maximum uptake diatoms at 0°C	1.50	d ⁻¹
RF_0	Maximum uptake flagellates at 0°C	0.75	d ⁻¹
S_{DIA}	Sinking rate diatoms	-1	m d ⁻¹
$Iopt_{dia}$	Optimum PAR diatoms	95	W m ⁻²
$Iopt_{flag}$	Optimum PAR flagellates	105	W m ⁻²
k_c	Attenuation constant self-shading	0.03	m ² (mg Chl a) ⁻¹
LPN	Loss rate phytoplankton to nutrients at 0°C	0.03	d ⁻¹
LPD	Loss rate phytoplankton to detritus at 0°C	0.02	d ⁻¹
Ths_1	Half-saturation temperature diatoms	12	°C
Ths_2	Half-saturation temperature flagellates	7	°C
Q_{10}	Maintenance temperature coefficient	0.07	°C ⁻¹
RFR	Redfield ratio N:P (mol-based)	16:1	fraction
N:Si	Si:N-ratio (mol-based)	1:1	fraction
Zooplankton			
$Imax_{MEZ}$	Maximum grazing mesozooplankton at 12°C	0.47	d ⁻¹
$Imax_{MIZ}$	Maximum grazing microzooplankton at 0°C	0.60	d ⁻¹
K_{MEZ}	Half-saturation ingestion mesozooplankton	0.32	mmol-N m ⁻³
K_{MIZ}	Half-saturation ingestion microzooplankton	0.60	mmol-N m ⁻³
AE_{MEZ}	Assimilation efficiency mesozooplankton	0.65	fraction
AE_{MIZ}	Assimilation efficiency microzooplankton	0.60	fraction
R_{MEZ}	Active respiration mesozooplankton	0.29	fraction
R_{MIZ}	Active respiration microzooplankton	0.35	fraction
β_{MEZ}	Basal respiration mesozooplankton at 0°C	0.005	d ⁻¹
β_{MIZ}	Basal respiration microzooplankton at 0°C	0.03	d ⁻¹
$pref_{DI}$	Grazing preference for diatoms by MEZ and MIZ	1.0	fraction
$pref_{FL}$	Grazing preference for flagellates by MEZ and MIZ	1.0	fraction
$pref_{MIZ}$	Grazing preference for microzooplankton by MEZ	1.0	fraction
$Mmax_{MEZ}$	Maximum mortality mesozooplankton at 0°C	0.004	d ⁻¹
$Mmax_{MIZ}$	Maximum mortality microzooplankton at 0°C	0.030	d ⁻¹
KM_{MEZ}	Half-saturation mortality mesozooplankton	0.07	mmol-N m ⁻³
KM_{MIZ}	Half-saturation mortality microzooplankton	0.02	mmol-N m ⁻³
Ths_{MIZ}	Half-saturation temperature microzooplankton	4	°C
SVM_{MEZ}	Seasonal vertical migration mesozooplankton	0-25	m d ⁻¹
Detritus and nutrients			
DN	Mineralisation of detritus at 0°C	0.001	d ⁻¹
DN_{Si}	Mineralisation of Si-detritus at 0°C	0.0001	d ⁻¹

NI_0	Maximum nitrification rate at 0 °C	0.02	d^{-1}
K_{nit}	Oxygen half-saturation in nitrification	3.75	$mmol-O_2 m^{-3}$
K_{denit}	Nitrate half-saturation in denitrification	0.135	$mmol-NO_3 m^{-3}$
T_{sen}	Temperature coefficient on recycling processes	0.07	$^{\circ}C^{-1}$
$SEDR$	Sinking rate detritus	-20	$m d^{-1}$
RQN	Respiratory quotient in nitrification	2.0	$O_2:NO_3$
RQC	Respiratory quotient in detritus	1.0	$O_2:Organic-N$
S_{DET}	Settling rate detritus	20	$m d^{-1}$

961
962

963

964 **10.2 Appendix B, the ocean model (HYCOM)**

965 The ocean model (HYCOM) has 40 hybrid vertical levels, combining isopycnals with z-level
966 coordinates and sigma coordinates. Tides are included internally within the ocean model using
967 eight constituents and similar tides are added at the open boundaries using the Oregon State
968 University TOPEX/Poseidon Global Inverse Solution (TPXO 8.2,) Egbert and Erofeeva, 2002).
969 More than 100 rivers are included as monthly climatological discharges obtained from the
970 Global Runoff Data Centre (GRDC, <http://grdc.bafg.de>) and scaled as prescribed by Dai and
971 Trenberth (2002)(Dai and Trenberth, 2002). In addition the globally gridded Core v2 runoff data
972 (Large and Yeager, 2009) is added for Greenland, the Canadian Archipelago, Svalbard, and
973 islands within the Arctic Ocean.

974 The sea ice model (CICE) describes the dynamics and thermodynamics of the sea ice as
975 described by Rasmussen et al, 2018 (Rasmussen et al., 2018). The dynamics is driven by drag
976 from wind and ocean, surface tilt of the ocean, Coriolis force, and the internal strength of sea ice
977 that will resist movement of the ice pack. The internal strength is based on the Elastic-Viscous-
978 Plastic (EVP) sea-ice rheology (Hunke, 2001), that originates from the Viscous-Plastic (VP)
979 described by Hibler (1979)(Hibler, 1979). CICE includes 5 thickness categories of sea ice within
980 each grid cell in order to describe the inhomogeneity. The thermodynamics prescribes a vertical
981 temperature profile with a resolution of four sea ice layers and one layer of snow for each sea-ice
982 category (Bitz and Lipscomb, 1999). Snow is very important for the thermodynamics of sea ice
983 as it insulates sea ice from the atmosphere and has a higher albedo than sea ice. The lower
984 boundary is governed by the upper ocean temperature, which is usually the ocean freezing
985 temperature and is linearly dependent on its salinity. The upper boundary is governed by the heat
986 and radiation transfer between the atmosphere and the combined snow/ice surface. The net heat
987 flux is calculated based on the 2m atmospheric temperature, humidity, incoming long and short-
988 wave radiation, and 10m wind and the state of the surface of the sea-ice model.

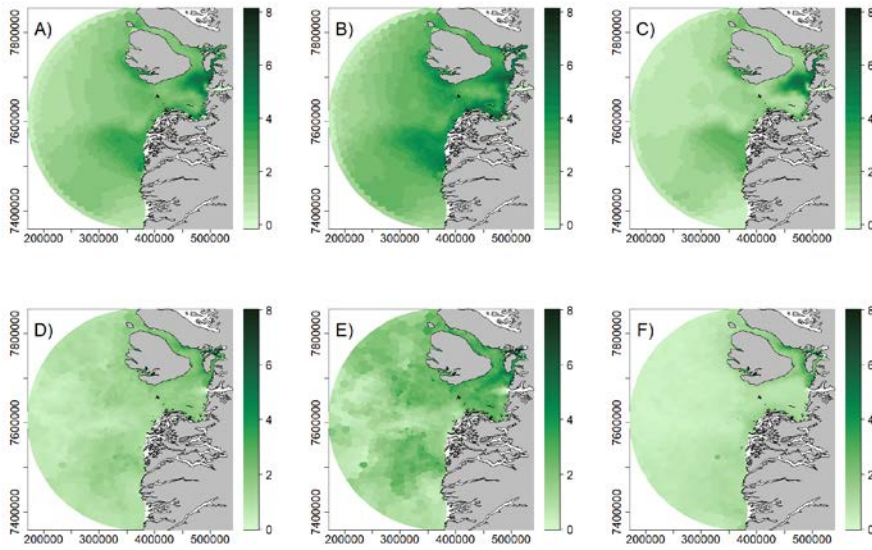
989 The HYCOM and CICE models used in this paper are coupled on each time step using the Earth
990 System modeling Framework (ESMF) coupler (Collins et al., 2004). The HYCOM-CICE set-up
991 at DMI used in this paper covers the Arctic Ocean and the Atlantic Ocean, north of about 20°S,
992 with a horizontal resolution of about 10 km (Madsen et al., 2016)..

993 The HYCOM-CICE model system assimilates re-analyzed sea-surface temperature
994 (<https://podaac.jpl.nasa.gov/GHRSST>, Høyer et al., 2012, 2014) and sea ice concentration
995 provided by the EUMETSAT Ocean and Sea Ice Satellite Application Facility (OSI SAF,
996 www.osi-saf.org, Lavergne et al., 2019) on a daily basis. The model is initialized in summer
997 1997 using the Polar Science Center Hydrographic Climatology (PHC; Steele et al., 2001) in the
998 Arctic Ocean and World Ocean Atlas 2001 0.25° (Conkright et al., 2002) in the Atlantic, with a
999 100 km linear transition. The atmospheric forcing is obtained from the Era-Interrim reanalysis
1000 (Dee et al., 2011) until 2017 and thereafter deterministic HRES ECMWF forcing
1001 (www.ecmwf.int).

1002 **10.3 Appendix C, Figures**

1003

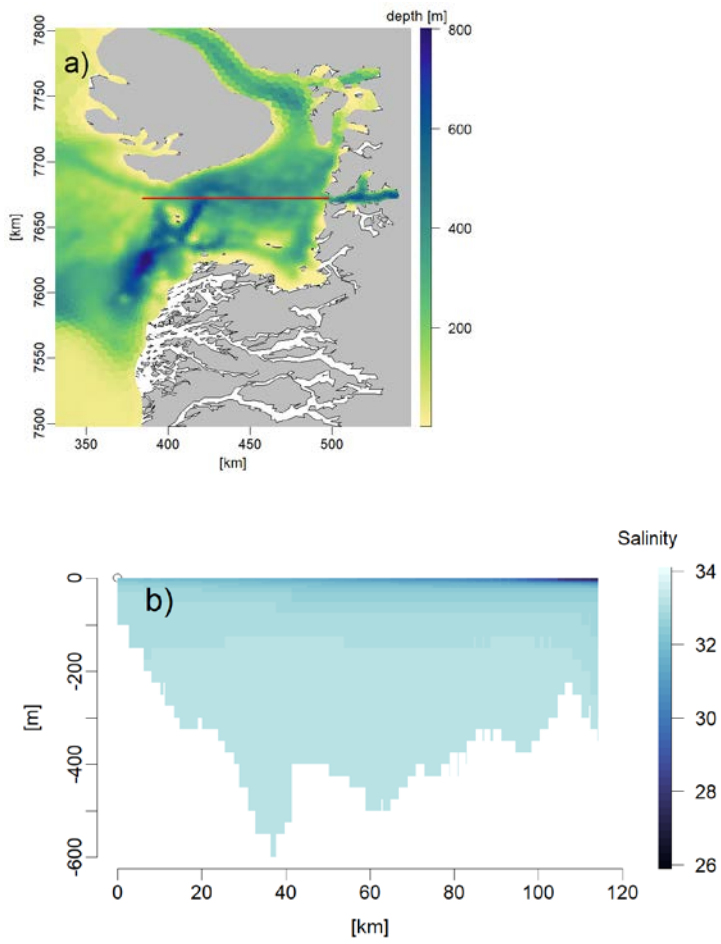
Figure C1: Surface Chl *a* concentration (mg chl *a* m⁻³) in 2010 obtained from the model (A-C) and from remote sensing (D-F). A) and D) are annual averages, B) and E) are April-June averages, and C) and F) are July-September averages.



1004

1005

Figure C2: a) Position and b) bathymetry of transect (x-axis: distance in km, y-axis: depth in m) shown in Figure C3.



1006

1007

Figure C3: Transects (x-axis: distance in km, y-axis: depth in m) of salinity (a, b) temperature ($^{\circ}\text{C}$) (c, d), DIN (mmol m^{-3}) (e, f), Chl *a* (mg m^{-3}) (g, h) and NPP ($\text{mgC m}^{-3} \text{d}^{-1}$) (i, j) in April (left) and August (right) 2010 along the transect shown in figure C2:

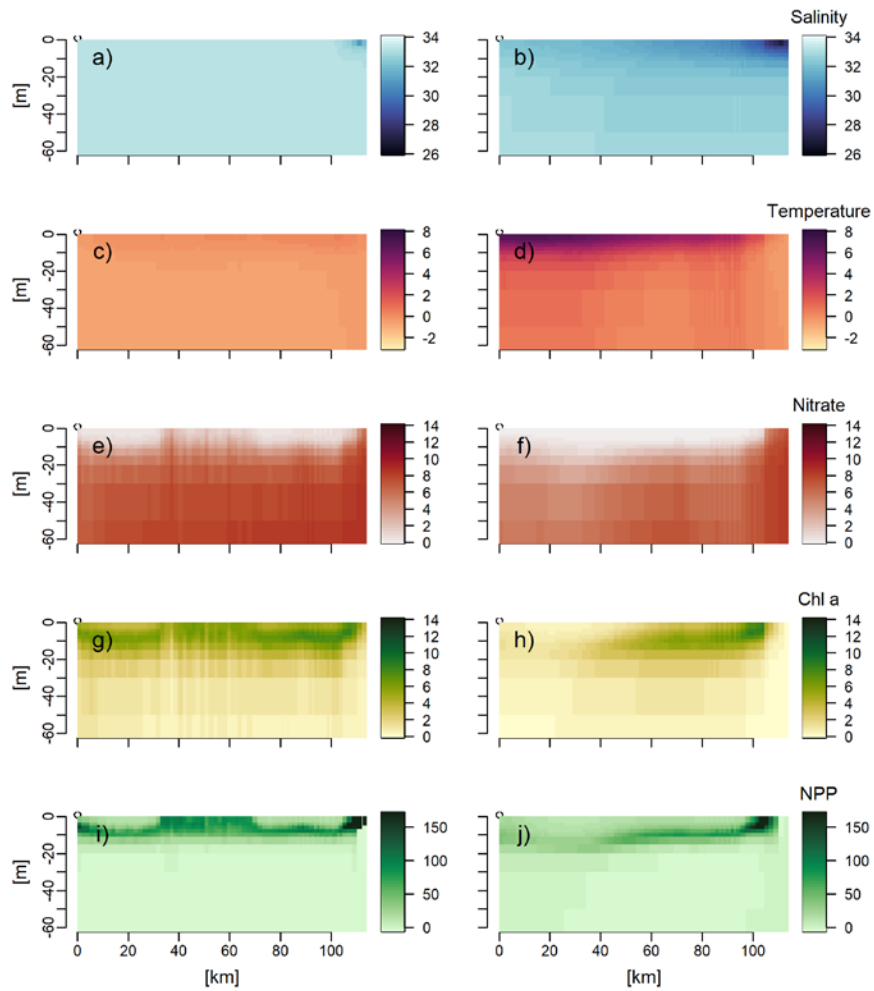


Figure C4. Vertical profiles of a) East-West velocities and b) vertical velocities at the ice edge in Jakobshavn Isbræ for 2010, the scenario noQNP, and the scenario with subglacial discharge at the glacier grounding line.

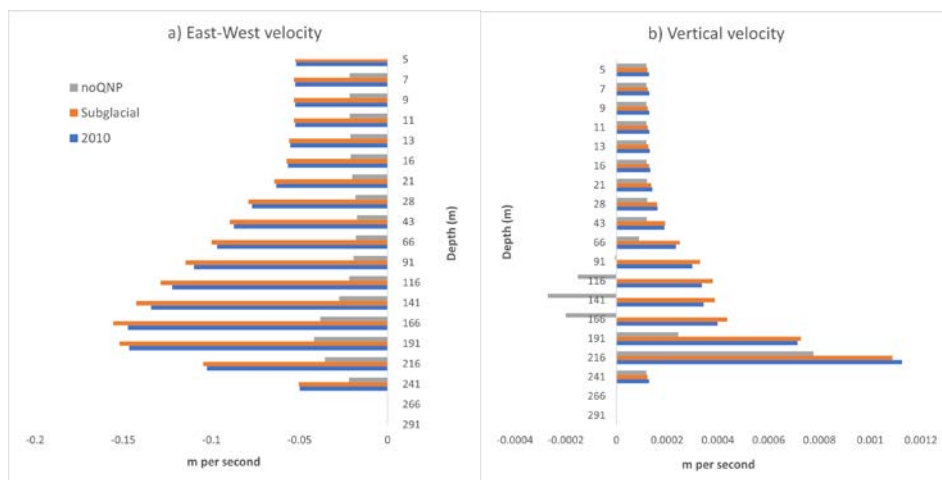
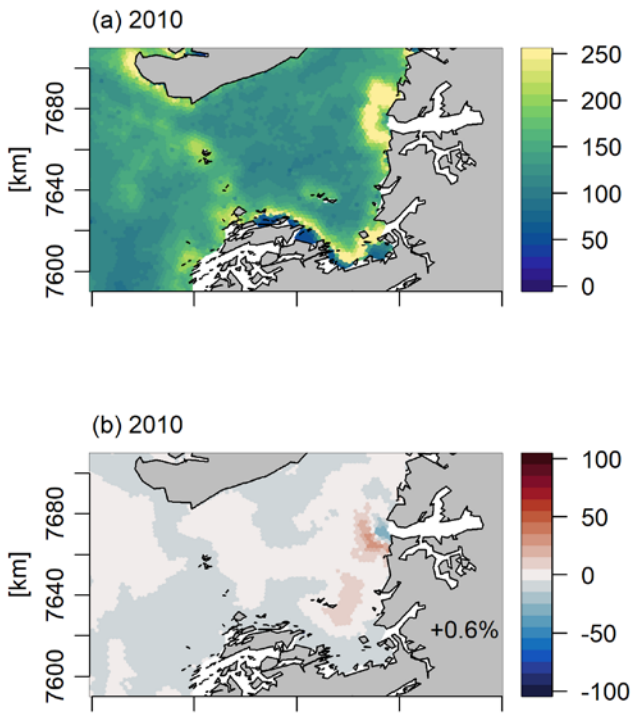


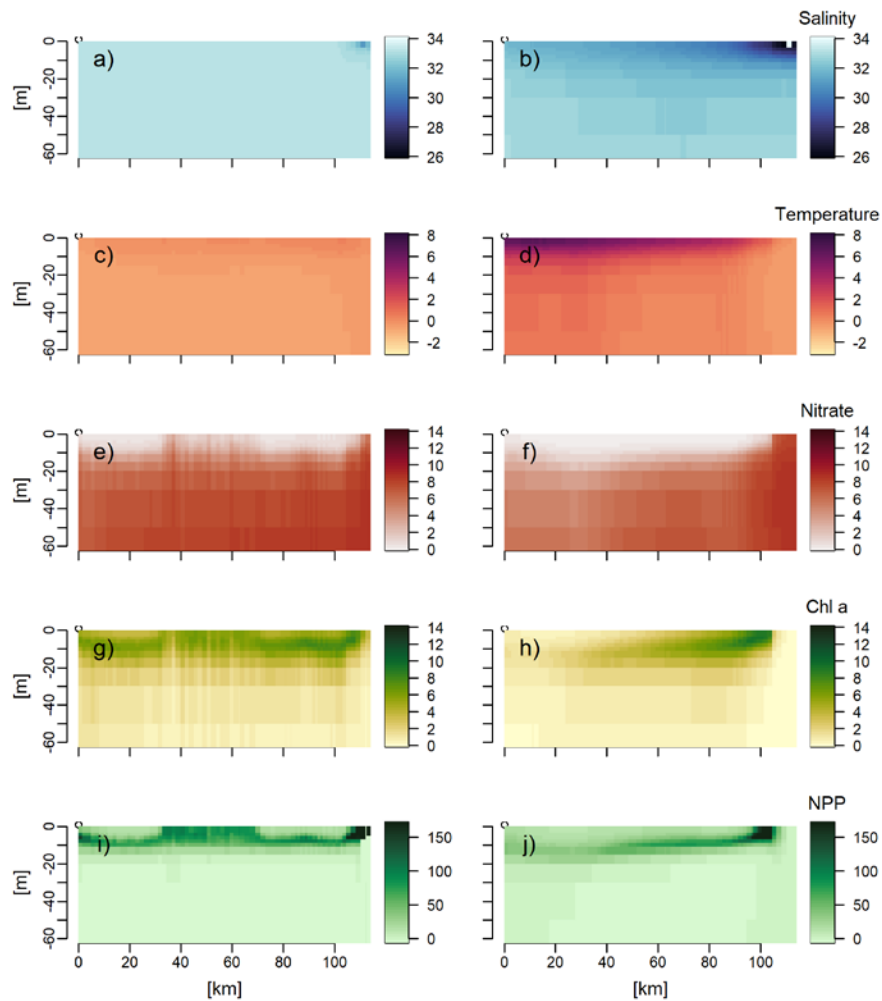
Figure C5: Annual primary production in 2010 (a) when the ice runoff is inserted at the glacier grounding line instead of in the surface as in the standard model run (Fig C3), and percentage change relative to the standard model run (b). The percentages in the bottom of the figure (b) are the changes in primary production in the total area shown.



1011

1012

Figure C5C6: Transects (x-axis: distance in km, y-axis: depth in m) of salinity (a, b) temperature ($^{\circ}\text{C}$) (c, d), DIN (mmol m^{-3}) (e, f), Chl *a* (mg m^{-3}) (g, h) and NPP ($\text{mgC m}^{-3} \text{d}^{-1}$) (i, j) in April (left) and August (right) 2010 along the transect shown in figure C2 when the ice runoff is inserted at the glacier grounding line instead of in the surface as in the standard model run (Fig C3).



1013

1014

